Host immune response against the emerging fungal pathogen *Candida auris*: transcriptional and functional insights

Mariolina Bruno[#1], Simone Kersten[#1, 2], Judith M. Bain[3], Martin Jaeger[1], Michael D. Kruppa[4], Douglas W. Lowman[4], M. Zuchao[4], Y. Ning Jiao[4], Anuradha Chowdhary[5], George Renieris[7], Frank L. van de Veerdonk[1, 6], Bart-Jan Kullberg[1, 6], Evangelos J. Giamarellos-Bourboulis[7], Alexander Hoischen[1, 2], Neil A. R. Gow[3, 8], Alistair J. P. Brown[3, 7], Jacques F. Meis[6, 9], David L. Williams[4, *], Mihai G. Netea[1,10, *]*

[1] Department of Internal Medicine, Radboud Institute for Molecular Life Sciences, Radboud University Medical Center, Nijmegen, the Netherlands
[2] Department of Human Genetics, Radboud Institute for Molecular Life Sciences, Radboud University Medical Center, Nijmegen, the Netherlands
[3] Medical Research Council Centre for Medical Mycology, University of Aberdeen, Foresterhill, Aberdeen, UK
[4] Departments of Surgery and Biomedical Sciences and Center of Excellence in Inflammation, Infectious Disease and Immunity, Quillen College of Medicine, East Tennessee State University, Johnson City, TN, USA
[5] Department of Medical Mycology, Vallabhbhai Patel Chest Institute, University of Delhi, New Delhi, India
[6] Center of Expertise in Mycology, Radboud University Medical Center and Canisius Wilhelmina Hospital, Nijmegen, the Netherlands
[7] 4th Department of Internal Medicine, National and Kapodistrian University of Athens, Medical School, Athens, Greece.
[8] School of Biosciences, University of Exeter, Exeter, UK.
[9] Department of Medical Microbiology and Infectious Diseases, Canisius Wilhelmina Hospital, Nijmegen, the Netherlands
[10] Lead Contact

[#]These authors contributed equally

**These authors share senior authorship*

Corresponding author:

Mihai G. Netea

Department of Internal Medicine (463) and Radboud Center for Infectious Diseases (RCI), Radboud University Nijmegen Medical Centre, Geert Grooteplein 8, Nijmegen 6500 HB, the Netherlands. mihai.netea@radboudumc.nl

SUMMARY

Candida auris is the most important emerging fungal pathogen, yet insights into the mechanisms underpinning its immune recognition and control are lacking. Here, we integrate transcriptional and functional profiling of immune cells to uncover anti-*C. auris* defense mechanisms. *C. auris* induces stronger cytokine responses than *C. albicans*, but has a lower macrophage lysis capacity. *C. auris* innate immune activation is induced through recognition of C-type lectin receptors and Syk-/Akt-dependent pathways. In particular, triggered by mannan structures that have previously gone undescribed. In a murine model of disseminated candidiasis, *C. auris* was less virulent than *C. albicans*. Collectively, *C. auris* is a strong inducer of anti-fungal innate host defense and the intrinsic virulence of *C. auris* is not higher than that of *C. albicans*. This suggests the main challenges in controlling this new pathogen lie in effective infection control measures and antifungal drug resistance, rather than high virulence and immune escape.

INTRODUCTION

Candida auris is an important emerging fungal pathogen that was first described in 2009, and has, since then, spread across five continents as a causative microorganism of hospital-acquired infections (Meis and Chowdhary, 2018). For several reasons, *C. auris* is one of the most challenging of emerging human pathogens identified in the last decade. It is highly resistant to many of the commonly used antifungal drugs (Chowdhary et al., 2018), and has rapidly spread worldwide within a few years (Clancy and Nguyen, 2017) through the nearly simultaneous (but independent) emergence of four distinct phylogeographical clades (Lockhart et al., 2017). *C. auris* poses difficulty in routine microbiological identification (Kathuria et al., 2015, Mizusawa et al., 2017) and is challenging to eradicate in healthcare settings (Ruiz-Gaitan et al., 2018, Schelenz et al., 2016, Vallabhaneni et al., 2017, Lee et al., 2011). This is due to its strong capacity to colonize skin, its transmittance via patient-to-patient contact or contaminated fomites, and its high survival capacity on plastic surfaces (Welsh et al., 2017). The risk factors for *C. auris* infections are generally similar to those for other types of *Candida* infections, such as hospitalization, use of central venous catheters, abdominal surgery and exposure to broad-spectrum antibiotics or antifungals (Rudramurthy et al., 2017). However, due to its intrinsic resistance to many anti-mycotic drugs, the overall crude mortality rate of *C. auris* candidemia is high ranging from 30% to 60%, with infections typically occurring several weeks (10-50 days) after admission (Schelenz et al., 2016, Lockhart et al., 2017, Mohd Tap et al., 2018, Chowdhary et al., 2017).

Considering the importance of *C. auris* as an emerging human pathogen, it is imperative to understand the host defense mechanisms that protect against it. This is particularly true given the high resistance of this fungus to anti-mycotic drugs, which makes it a prime candidate for the development of host-directed therapy (i.e. immunotherapy). However, almost nothing is known regarding the host immune response against *C. auris*. Host defense against *Candida* species is dependent on a finely tuned interplay of innate and adaptive immune responses. A first, physical barrier, consists of the skin and mucosa. The second barrier, presented by the innate immune system, is largely dependent on the recognition of evolutionarily conserved fungal cell wall components (pathogen-associated molecular patterns, PAMPs) by innate immune cells such as monocytes, macrophages and neutrophils. In turn, the release of proinflammatory cytokines, combined with antigen-presentation activity of myeloid cells, is crucial for shaping the adaptive immune immunity, representing a third, longer term barrier against fungal infection (Richardson and Moyes, 2015).

The *Candida* cell wall is divided into an outer layer of highly mannosylated proteins (mannoproteins) and an inner layer, mainly comprised of β(1,3) and β(1,6)-glucans and chitin (Erwig and Gow, 2016). These PAMPs are recognized by various pattern recognition receptor (PRRs) on the surface of immune cells: C-type lectin receptors (CLRs) such as Dectin-1, Dectin-2, MMR (macrophage

mannose receptor), Mincle (macrophage-inducible C-type lectin), DC-SIGN (dendritic cell specific intercellular adhesion molecule-3-grabbing non-integrin) and Toll-like Receptors (TLRs), especially TLR2 and TLR4 (Gow et al., 2011). Coordinated engagement of PRRs results in the activation of innate immune effector mechanisms such as phagocytosis, the release of reactive oxygen species (ROS) and production of pro- and anti-inflammatory cytokines. In turn, together with the antigen-presentation activity of myeloid cells, the release of pro-inflammatory cytokines shape the adaptive immune response (Richardson and Moyes, 2015).

While these antifungal host defense mechanisms have been extensively studied for *C. albicans,* very little is known about host immune response against *C. auris*. Almost all multi-drug resistant *C. auris* strains are susceptible to killing by the salivary antimicrobial peptide Histatin 5 (Hst-5) (Pathirana et al., 2018), while Johnson and colleagues showed that neutrophil recruitment and formation of neutrophils extracellular traps (NETs) were lower for *C. auris* than *C. albicans* (Johnson et al., 2018). Recently it was reported that *C. albicans, C. tropicalis, C. guilliermondii, C. krusei* and *C. auris* differentially stimulate cytokine production in peripheral blood mononuclear cells (PBMCs) (Navarro-Arias et al., 2019), but little is known regarding the particularities of these responses and the mechanisms mediating them. Considering the knowledge gap in our understanding of anti-*C. auris* host defense mechanisms, we set out to comprehensively assess the mechanisms through which innate immune cells recognize *C. auris,* initiate innate antifungal immune responses, and protect the host against *C. auris* infection. This mechanistic insight into *C. auris* host interactions should facilitate the development of novel host-directed approaches for the treatment of severe *C. auris* infections and, thereby, improve patient outcomes.

RESULTS

Common and specific transcriptome signatures induced by *C. albicans* and *C. auris* in human immune cells

To gain a broad overview of the immune cell response against *C. auris*, RNA sequencing was performed on PBMCs from three healthy donors that were exposed to either live *C. albicans* or *C. auris* for 4 or 24 hours. *C. albicans* was included as a reference species as it remains the most common cause of mucosal and systemic candidiasis (Brown et al., 2012).

Principle component analysis (PCA) of the PBMC transcriptome-data revealed that the majority of the variance in the dataset was time-dependent (Figure S1A), demonstrated by clear separation of the 4 hour and 24-hour stimulation time points. At 4 hours, clustering of the donors

irrespective of stimulus reflects inter-individual differences to underpin the observed variance, whereas at 24 hours the response is primarily stimulus-driven (Figure S1B), indicated by the distinct clustering and scattering of donor responses dependent on pathogen exposure. After 4-hour stimulation, PBMCs stimulated with live *C. albicans* and *C. auris* cluster together, suggesting significant overlap between short-term responses of PBMCs to these two *Candida* species. As PBMC donors were considered biological replicates, comparison of the average PBMC response to their control condition revealed significant overlap in the 4-hour host response between *C. albicans* and *C. auris*. With 71 differentially expressed genes (DEG; fold change ≥2 and p-adjusted value <0.01) upregulated by both *Candida* species, the respective overlap ranges from 67% of the total number of DEG for *C. albicans* (71 / 109), to 95% of the total number of DEG for *C. auris* (71 / 79).

At a later phase 24h after stimulation, the common *C. auris*- and *C. albicans*-induced host response increased to 243 DEG (Figure 1), in turn accounting for 55% of the total number of DEG for *C. albicans* (243 / 441) and 50% of the total number of DEG for *C. auris* (243 / 484). This late phase decreased overall shared response between both *Candida* species, was consistent with the observation that the 24-hour induced PBMC transcriptomes were more stimulus-specific (Figure S1B). Pathway enrichment analysis revealed that the 4-hour *Candida* intrinsic response can be delineated by a common activation of the CC and CXC chemokines (Table S2). The 24-hour PBMC transcriptomic response was characterized by a broader upregulation of chemokines, interleukins, tumor necrosis factor and their receptors (Figure 1, Table S3).

The substantial activation of glucose, fructose and mannose metabolism was unique to the *C. albicans*-induced transcriptional response of PBMCs at 24 hours. Conversely, DEG observed to be stronger induced upon PBMC exposure to *C. auris* appeared to be linked to type I and II interferons, as well as antiviral mechanisms triggered via IFN-stimulated genes, including the ISG15 antiviral mechanisms (Figure 1, Table S3). Collectively, these data show that *C. albicans* and *C. auris* are potent activators of the immune system in the host, and they are able not only to activate common transcriptional responses, but also induce pathways specific to each pathogen.

C. auris is a more potent inducer of host immune response compared to *C. albicans*

In contrast to *C. albicans*, one third of the top 15 enriched pathways based on DEG unique for *C. auris* were also found to be enriched in the common *Candida* response (Figure 1). This indicates that *C. auris* has the ability to upregulate more genes in these pathways compared to *C. albicans*. Most pronounced within these unique DEG were distinct interleukins such as *IL1RN* (encoding for IL-Ra),

IL10, *IL19*, *IL26* and *IL27*, as well as interferon (IFN) associated genes, e.g. *STAT2, DDX58, EIF2AK2, OAS2, OAS3, IFIT2, IFIT3, IFIT35* and *IFITM1* (Table S3). Furthermore, DEG were more potently induced in response to *C. auris* than *C. albicans* (Student's T-test, p-value of 0.003). An additional pathway enrichment analysis on all upregulated DEG confirmed that the total number of DEG for mutually enriched pathways was higher when the PBMCs were stimulated with *C. auris* rather than with *C. albicans* (Figure S1C). Collectively, the broader and stronger induction of DEG by *C. auris* resulted in higher enrichment scores (q-value) for corresponding pathways in comparison to *C. albicans*, suggesting that *C. auris* is a more potent trigger of the host response.

With the transcriptomic analysis suggesting cytokine signaling to be at the core of the host response, we aimed to verify these observations on protein level. For this, the cytokine production of PBMCs isolated from healthy volunteers was assessed following exposure to three different clinical live *Candida* isolates. All cultured under similar conditions, the cytokine production was assessed after 24 hours. With the exception of the anti-inflammatory IL1-Ra, PBMCs exposed to both clinical isolates of *C. auris* for 24 hours produced significantly more pro-inflammatory cytokines TNF-α, IL-6 and IL-1β compared to the *C. albicans*-stimulated PBMCs (Figure 2A). These findings are in line with our observations at the transcriptional level, where the PBMCs stimulated with *C. auris* were observed to induce a higher expression of *IL-6* ($Log_2FC = 8.41$) and *IL-1β* ($Log_2FC = 6.45$) than upon exposure to *C. albicans* ($Log_2FC = 7.58$ for *IL-6*; $Log_2FC = 5.59$ for *IL-1β*) (Figure S2A).

C. auris replicates faster than *C. albicans in vivo,* leading to altered multiplicity of infection (MOI), but does not cause macrophage lysis

An important line of defense against *Candida* infections is the killing of fungal cells by professional phagocytes of the innate immune system, such as monocytes, macrophages or dendritic cells. In order to study the differences in phagocytosis dynamics of professional phagocytes between *C. auris* and *C. albicans,* we employed live-cell video microscopy coupled with dynamic image analysis of bone marrow-derived macrophages (BMDMs). Phagocytosis was assessed by combining BMDMs with live and thimerosal-killed *C. auris* and *C. albicans* strains at an intended MOI of 3:1, yeast cells per macrophage. By including fixed yeasts, we were able to assay phagocytosis in the absence of rapid changes in the composition of the *Candida* cell wall. Results were expressed as percentage of phagocytic BMDM (% uptake), indicating the percentage of macrophages having phagocytosed at least one fungal cell. In addition, we assayed the Phagocytic Index which is defined as the number of fungal cells engulfed per 100 macrophages. No significant differences in *C. auris* and *C. albicans* phagocytosis (% uptake) were observed for fixed *Candida* (Figure 2C). However, one of the live *C. auris* strains

(10051893) had a lower phagocytosis efficiency compared to the other strains (Figure S3B). There was a trend towards a higher phagocytic index in BMDMs at later time points (after the second hour) for both of the fixed *C. auris* strains (Figure 2C), possibly because fungal cells were phagocytosed in clusters. Focused on live strains, we observed that the engulfment of both *C. auris* strains resulted in a higher phagocytic index at later time points, especially after 3 hours (Figure S3A).

Using live cell microscopy, live *C. auris* cells were observed to bud repeatedly outside the macrophages, at a rate of doubling of circa 1-hour. The *C. auris* budding rate decreased following phagocytic engulfment, although cells continued to multiply within phagosomes (Video S1). Of interest, *C. auris* 10051895 accumulated in high numbers within macrophages, indicating that the starting MOI had exceeded the intended initial 3:1 ratio (Video S2). This led us to look at the actual MOI ratios observed from videos at the start of image acquisition, which could be as high as 9:1 and 11:1 for *C. auris*. We deduced that the delay time between counting the *Candida* in each sample until starting the imaging led to greater numbers of *C. auris* cells, presumably due to ongoing budding, despite storage of samples at 4°C in PBS until the live imaging commenced. In contrast, the MOIs for *C. albicans* remained around the desired target of 3:1 yeast:macrophage.

The elevated MOIs for *C. auris* may be a contributing factor to the high phagocytic index achieved at 3 hours for strain 10051895 (Figure S3B). However, an elevated starting MOI for *C. auris* 10051893 did not enhance phagocytosis, as this live strain was poorly recognized by BMDM. From the representative movies recorded we quantified the distribution of yeast per individual macrophage after 3 hours and found that for both *C. auris* strains, there was a tendency for some macrophages to engulf many cells, yet for other macrophages to engulf none. This phenomenon was less surprising for the *Candida* experiments using live microorganisms (Figure S3C), because *C. auris* continues to divide prior to and during the phagocytosis experiment. However, the fixed strains also displayed this varied distribution, with both strain of *C. auris* being phagocytosed in great numbers by some macrophages (Figure 2D). Supplementary video 3 shows it is possible to observe that *C. auris* cells are taken up extensively into a subpopulation of macrophages, but despite the vast burden, these phagocytes continue to move around in pursuit of further fungal targets.

Finally, macrophage lysis was determined following engulfment of live *Candida* (Figure 2E) and it emerged that the *C. auris* strains examined were less able to kill macrophages after 3 hour than *C. albicans* (Video S4), despite having a comparable (or greater, in the case of *C. auris* 10051895) phagocytic index. These findings demonstrate that *C auris* is differentially recognized by phagocytic BMDMs and internalized with a higher phagocytic index compared to *C. albicans*, but is not able to induce lysis of the phagocytic cells.

Host immune response upon *C. auris* exposure is mediated through heat-sensitive cell wall components

Differential surface structures such as mannoproteins, or enhanced exposure of β-glucans in the *C. auris* and *C. albicans* cell walls, could account for the differential cytokine responses triggered by these pathogens. To elucidate which of these components might be more important, we heat-killed *C. auris* and *C. albicans* strains, a procedure that denatures surface mannoproteins, but not the β-glucans. The heat-killed strains were used to stimulate PBMCs for 24 hours and 7 days. Since the production of reactive oxygen species (ROS) can positively contribute to immune responses (Klebanoff, 2005), ROS production in both neutrophils and PBMCs was assessed, together with the pro-inflammatory cytokine production of PBMCs.

In both neutrophils and PBMCs (**Figure S3D,S3E**) the ROS production upon stimulation with opsonized heat-killed *C. auris* strains was observed significantly lower than in *C. albicans*. More surprising, in PBMCs stimulated with heat-killed *C. auris* the cytokine response was almost completely lost after 24 hours compared to heat-killed *C. albicans* (IL-1β, IL-6, TNF-α, IL-1Ra; **Figure 2B**, **S2C**) and live *C. auris* (**Figure 2A**). Furthermore, after 7 days, the production of IFN-γ, IL-17 and IL-22 by PBMCs stimulated with heat-killed *C. auris* was significantly lower compared to heat-killed *C. albicans* (**Figure S2D**). Hence, we reasoned that a heat sensitive component of the cell wall might be responsible for most of the increased cytokine induction by *C. auris*.

Mannans drive the host response to *C. auris*

We attempted to unravel the contribution of the different fungal cell wall components to the activation of host responses by *C. auris,* compared to *C. albicans.* PBMCs were exposed to the purified cell wall components, β-glucans and mannans, from both *Candida* species, and the transcriptional responses of the stimulated immune cells were assessed by RNA sequencing. The species-specific cell wall contribution was assessed by comparison of the number of shared DEG upon exposure to the different cell wall components and expressed as proportion of the respective live stimulus.

The early 4-hour host response was predominantly induced by β-glucan, which was sufficient to explain around 82% and 57% of the respective live responses of *C. albicans* (89 / 109) and *C. auris* (45 / 79) (**Figure 3A**). The β-glucans from each species resulted in similar PBMC stimulation profiles (**Figure 3B**). Although the relative contribution of *C. albicans* β-glucan decreases to approximately 13% (55 / 441) in the late phase, 24 hours after stimulation, they remain able to upregulate several *C. albicans*' top 50 DEG, leaving them a main contributor of the evoked response in the live setting (**Figure 3A**, **3B**). In contrast, β-glucans from *C. auris* failed to elicit a response analogous to the live *C.*

auris exposure, explaining only a mere 2% (10 / 484) of the live *C. auris*-induced response. Conversely, however, mannans from *C. auris* stimulated 28% (136 / 484) of the evoked transcriptional response to live *C. auris* cells. Moreover, *C. auris* mannan seemed to outperform *C. albicans* β-glucan in relation to the top 50 DEG of *C. albicans*, displaying an induction pattern similar to its live setting (**Figure 3B**). Overall, these results indicate that the host recognition and subsequent initiation of downstream responses against *C. albicans* is mainly dependent on β-glucan. For *C. auris*, early 4-hour stimulation of PBMCs is mainly mediated by β-glucan, whereas mannans are fundamental for orchestrating the *C. auris*-specific host response at later time points (24 hours).

Our data suggest a stronger *C. auris* host immune response and a differential role in gene expression between *C. albicans* and *C. auris* cell wall components. Therefore, to investigate the differences in cell wall structure between *C. auris* and *C. albicans*, we first compared forward (FSC) and side (SSC) light scatter of fungal cells using flow cytometry. In line with what has been previously been described (Larkin et al., 2017), we found that the *C. auris* strains have a smaller average cell size compared to *C. albicans*. Of the *C. auris* strains, strain 10051893 shows more complexity/granularity (higher SSC) than strain 10051895 (**Figure 4A**).

Next, we measured β-glucan exposure on the fungal cell surface by flow cytometry on thimerosal-fixed *Candida* cells stained with Fc-Dectin-1. Both *C. auris* strains displayed significantly reduced exposure of β-glucan as compared to *C. albicans* (**Figure 4B**). At the gene expression level, *C. auris* β-glucan were less effective to induce IL-1Ra gene expression as compared to β-glucan isolated from *C. albicans* (**Figure S2A**). At the cytokine level, though large variation between different strains was observed, no significant differences in cytokine production of PBMCs stimulated with purified β-glucans from *C. auris* compared to *C. albicans* were found (**Figure 4C**). Moreover, similarly to *C. albicans* β-glucan, *C. auris* β-glucan synergistically boosted Pam_3cys (TLR2 agonist)-induced IL-1β production in PBMCs (**Figure 4F**), as well as TNF-α and IL-6 production (**Figure S4D**). This observation is supported by the similar chemical structure of *C. auris* and *C. albicans* β-glucan in terms of branching and length (Williams *et al.*, unpublished data). These data argue strongly that the higher cytokine production by PBMCs upon *C. auris* stimulation was not due to differences in the chemical properties of *C. auris* β-glucan.

Having ruled out a major role for β-glucans in explaining the difference in cytokine stimulation induced by *C. auris* and *C. albicans*, we assessed the role of glycosylated mannoproteins from the fungal cell wall (Hall and Gow, 2013a). *C. auris* mannans have a unique structure with low molecular weight and side chains that have never been observed before in fungi (**Figure 4E**). Examination of mannan exposure, by staining thimerosal-fixed *Candida* cells with Concanavalin A (ConA), revealed a

relatively low level of exposure of surface mannans in *C. auris* (Figure 4B), which is probably linked to their smaller cell size. However, in contrast with *C. albicans* mannans, these *C. auris* mannans significantly upregulated expression of *IL-6*, *IL-1β* and *IL-1Ra* genes in PBMCs (Figure S2B).

In line with these observations, mannans from all eight *C. auris* strains induced a significantly higher cytokine production than *C. albicans* mannans 24 hours after stimulation of PBMCs (Figure 4D). Opsonization by human serum was necessary for mannan-induced production of cytokines (Figure 4G and S4A). After 7 days of stimulation, mannans from *C. auris* were also capable for inducing a Th-dependent cytokine production, such as IFN-γ, IL-17 and IL-22 (Figure S4B and S4C),

The CLRs complement receptor 3 (CR3) and MMR are crucial for immune recognition of *C. auris* and subsequent cytokine production in an Akt-, Syk- and Raf-1-dependent manner.

In the following set of experiments, we investigated the pattern recognition receptors (PRR) and intracellular pathways involved in the recognition of *C. auris* and the subsequent activation of the immune system. The serine/threonine-protein kinase AKT mediates signals downstream of several TLRs and CLRs (Brown et al., 2011). Interestingly, the Akt/PI3K inhibitor wortmannin drastically decreased the induction of the inflammatory cytokines, TNF-α, IL-6 and IL-1β, 24 hours after exposure to *C. auris* (Figure 5A, S5D). In addition, inhibition of Syk and Raf-1 (Gringhuis et al., 2009) also decreased TNF-α, IL-6 and IL-1 β production in response *C. auris* stimulation (Figure 5B, S5E), indicating the involvement of these two signaling pathway in cytokine production.

Due to the importance of Syk and Akt pathways for mediating signaling through CLRs, we subsequently hypothesized a role for these receptors in *C. auris* recognition. Therefore, we pre-incubated PBMCs with neutralizing antibodies against important *Candida* CLRs (e.g. Dectin-1, Dectin-2, Mincle, DC-SIGN, MMR, CR3 and their control isotypes), 1 hour prior to stimulation with live *C. albicans* or *C. auris*. We observed a significant reduction in *C. auris*-induced IL-6 production upon blocking of MMR (Figure 5C). Interestingly, we observed a significant increase in IL-6 production after DC-SIGN and Dectin-1 blockade (Figure 5C). Blockade of CR3 led to a significant reduction in IL-1β production (Figure 5C) and an increase in IL-1Ra production (Figure S5C).

In order to evaluate the role of CLRs in the Th-derived cytokine production against *C. auris,* we stimulated PBMCs for 7 days with either heat-killed *C. albicans* or *C. auris* in the presence of the blocking PRR antibodies or the isotype controls and of the pathway inhibitors or their vehicle. CR3 blockade led to a significant reduction in IFN-γ production (Figure 5D). In contrast, IL-17 and IL-22

production was not influenced by blockade of Mincle, CR3 and MMR, or after the inhibition of AKT, SYK and Raf-1 signaling pathways (Figure 5D-E).

C. auris is less virulent than *C. albicans* in an experimental model of murine disseminated candidiasis

In order to evaluate the virulence of *C. auris in vivo*, immunocompetent C57BL/6J mice were injected intravenous (i.v.) with either 10^7 CFU of *C. auris* or *C. albicans*. Their survival was monitored over the course of 14 days, and fungal burdens in target organs was assessed. Significantly more immunocompetent mice survived infection with *C. auris* than with *C. albicans* (Figure 6A) and for *C. auris*, there was a correspondingly lower fungal burden in organs after 3 and 7 days (Figure 6B).

DISCUSSION

In this study we investigated the transcriptional and functional responses of human PBMC and murine BMDM to *C. auris*. We compared these responses to those elicited by *C. albicans*, the most frequent cause of nosocomial fungal infections in humans. *C. auris* induced a stronger immune response than *C. albicans* in human primary immune cells, an effect mediated by mannans with a unique chemical structure. This increased stimulation of the immune response was followed by lower virulence in a model of murine disseminated infection.

Because *Candida* induction of cytokine responses is mainly mediated by cell wall components, and especially β-glucans and mannans (Gow et al., 2007), we explored their distinct roles in the induction of the host immune response via integration of both transcriptomics and cytokine measurements. Firstly, *C. auris* induced robust transcriptional changes in human PBMCs. These included both common pathways induced by *C. albicans* as well, but also more robust specific IFN–dependent transcriptional programs and explicit cytokine responses. This conclusion is supported by a recent study by Mora-Montes and colleagues (Navarro-Arias et al., 2019). Secondly, *C. auris* cells appear to induce stimulation of immune cells by sequential engagement of different components of the cell wall. The early (4 hour) responses are mainly induced by β-glucans, and this initial phase of the response is largely similar to that induced by *C. albicans*. This is probably explained by the similar structure of *C. auris* and *C. albicans* β-glucans. In contrast, the late transcriptomic responses (24 hour) induced in PBMCs by *C. auris* display significant differences and broader upregulation of immune genes compared with those induced by *C. albicans*. These late responses are mainly mediated by *C.*

auris mannoproteins with a specific structure that include a unique M-α-1-phosphate side chain in the acid lable portion of C*. auris* mannans, which has not been observed in the fungal kingdom to date.

Thirdly, an important question concerns the PRRs responsible for the recognition of *C. auris.* Experiments using antibodies that block specific receptors revealed an important role for the CLRs, especially MMR and CR3 in the induction of cytokines by *C. auris*. The role of these receptors in the recognition of mannans is well known (Hall and Gow, 2013b). As expected, their inhibition led to partial loss of cytokine production, arguing that additional mannan-recognizing receptors contribute to anti-*C. auris* host defense. In addition to these receptors, pharmacological inhibition of common signaling pathways induced by CLRs show that AKT, SYK and RAF-1 pathways are all involved in *C. auris*-induced cytokine production. Additional studies are needed to elaborate these molecular mechanisms in detail, and identify other potential PRRs important for the recognition of *C. auris.*

Cytokine induction is important upon pathogen recognition, but the induction of phagocytosis is also crucial (Keppler-Ross et al., 2010). We observed a higher phagocytic index for *C. auris* compared to *C. albicans*. This is likely due to a better recognition of *C. auris* mannans by immune cells, as cell wall glycosylation is critically important for the recognition and ingestion of *C. albicans* by macrophages (McKenzie et al., 2010). Therefore, to shed more light on these processes, future investigations might examine the phagocytosis dynamics for *C. auris* mutant strains that are defective in their cell wall architecture. Interestingly, when the fate of the fungus was assessed through video time-lapse microscopy, it was also clear that the continued cell division of *C. auris* leads to altered MOI that are greater than *C. albicans* and this may also contribute to the stronger stimulation of inflammation. However, this did not result in the death of the phagocytes, most likely due to the lack of hypha formation by engulfed *C. auris* cells.

The stronger induction of cytokines and lower macrophage toxicity might have been expected to lead to lower virulence of *C. auris in vivo* compared with *C. albicans.* In line with this hypothesis, experiments in a model of murine disseminated candidiasis demonstrate that *C. auris* is less virulent compared to *C. albicans*, conclusion supported by a recent additional study (Fakhim et al., 2018, Ben-Ami et al., 2017). Neutrophils are considered one of the most important host immune response to fungi through phagocytosis and intracellular killing, or by releasing NETs (Urban and Nett, 2019). In a recent study (Johnson et al., 2018), human neutrophils were poorly recruited to sites of *C. auris* infection, were less able to kill *C. auris* compared to *C. albicans,* and they failed to form NETs in response *C. auris.* However, neutrophils are important contributors for the host defense against *Candida* species (Urban et al., 2006). Future studies are warranted to dissect the relative importance of neutrophils and macrophages in the host defense against *C. auris*.

In conclusion, we performed a first comprehensive assessment of the innate host defense mechanisms against the rapidly emerging human pathogen *C. auris*. The overall conclusion is that the host defense mechanisms induced by *C. auris* are generally recognizable antifungal mechanisms, but important specific responses are also triggered by unique *C. auris*-specific mannoprotein structures. The ensuing immune responses are effective and lead to an effective elimination of the fungus. Our study argues that the intrinsic virulence of *C. auris* is not higher than other *Candida* species circulating in the patient population: it is rather the hospital infection control profile of this pathogen and its high resistance to anti-mycotic drugs that make it dangerous. The identification of potent human anti-*C. auris* immune responses in humans opens on the other hand the door for the development of immunotherapeutic approaches to complement anti-mycotic therapy. The challenges that need to be pursued in the coming years are to identify in even more detail the most effective components of the anti-*C. auris* host defense, and design and test novel host-directed therapies to enhance these pathways and improve the outcome to the infection.

ACKNOWLEDGMENTS

We would like to thank Trees Jansen for performing the initial pilot experiments, Ilse Curfs-Breuker and Dirk Faro for their support at the CWZ hospital. We would like to thank Vinod Kumar for his input during the transcriptomic data analysis and Mark Gresnigt for the *in vitro* experimental suggestions. AJPB and NARG thank the MRC (MR/M026663/1) and Wellcome for support and the Medical Research Council (MRC) Centre for Medical Mycology at the University of Aberdeen (MR/N006364/1). A.H. and S.K. were supported by the Radboud Institute for Molecular Life Sciences. Part of the study was supported by the Hellenic Institute for the Study of Sepsis. D.L.W. was supported by National Institutes of Health grants NIH GM083016, GM119197 and C06RR0306551. M.G.N. was supported by an ERC Advanced Grant (no. 833247) and by a Spinoza Grant from the Netherlands Organization for Scientific Research.

AUTHOR CONTRIBUTIONS

Conceptualization, J.F.M., D.L.W., M.G.N.;

Methodology, M.B., S.K., J.M.B., M.J., M.D.K., D.W.L., M.Z., Y.N.J., A.C., A.H., N.A.R.G., A.J.P.B., J.F.M., D.L.W., M.G.N.;

Investigation, M.B., S.K., J.M.B., M.J, D.W.L., F.L.V., B.J.K., E.J.B., G.R., A.H, N.A.R.G, A.J.P.B., D.L.W. and M.G.N.;

Writing-original draft, M.B., S.K. and M.G.N.;

Writing- Review & Editing, M.B., S.K., J.M.B., M.J., M.D.K., D.W.L., M.Z., Y.N.J., A.C., F.L.V., E.J.B., A.H., N.A.R.G., A.J.P.B., J.F.M., D.L.W., M.G.N.;

Supervision: M.J., F.L.V., A.H., N.A.R.G, A.J.P.B. and M.G.N

DECLARATION OF INTERESTS

The authors declare no competing interests.

REFERENCES

ANDERS, S., PYL, P. T. & HUBER, W. 2015. HTSeq-a Python framework to work with high-throughput sequencing data. *Bioinformatics,* 31**,** 166-169.

BEN-AMI, R., BERMAN, J., NOVIKOV, A., BASH, E., SHACHOR-MEYOUHAS, Y., ZAKIN, S., MAOR, Y., TARABIA, J., SCHECHNER, V., ADLER, A. & FINN, T. 2017. Multidrug-Resistant Candida haemulonii and C. auris, Tel Aviv, Israel. *Emerg Infect Dis,* 23.

BROWN, G. D., DENNING, D. W., GOW, N. A., LEVITZ, S. M., NETEA, M. G. & WHITE, T. C. 2012. Hidden killers: human fungal infections. *Sci Transl Med,* 4**,** 165rv13.

BROWN, J., WANG, H., HAJISHENGALLIS, G. N. & MARTIN, M. 2011. TLR-signaling Networks: An Integration of Adaptor Molecules, Kinases, and Cross-talk. *Journal of Dental Research,* 90**,** 417-427.

CHOWDHARY, A., PRAKASH, A., SHARMA, C., KORDALEWSKA, M., KUMAR, A., SARMA, S., TARAI, B., SINGH, A., UPADHYAYA, G., UPADHYAY, S., YADAV, P., SINGH, P. K., KHILLAN, V., SACHDEVA, N., PERLIN, D. S. & MEIS, J. F. 2018. A multicentre study of antifungal susceptibility patterns among 350 Candida auris isolates (2009-17) in India: role of the ERG11 and FKS1 genes in azole and echinocandin resistance. *J Antimicrob Chemother,* 73**,** 891-899.

CHOWDHARY, A., SHARMA, C. & MEIS, J. F. 2017. Candida auris: A rapidly emerging cause of hospital-acquired multidrug-resistant fungal infections globally. *PLoS Pathog,* 13**,** e1006290.

CLANCY, C. J. & NGUYEN, M. H. 2017. Emergence of Candida auris: An International Call to Arms. *Clin Infect Dis,* 64**,** 141-143.

DOBIN, A., DAVIS, C. A., SCHLESINGER, F., DRENKOW, J., ZALESKI, C., JHA, S., BATUT, P., CHAISSON, M. & GINGERAS, T. R. 2013. STAR: ultrafast universal RNA-seq aligner. *Bioinformatics,* 29**,** 15-21.

ERWIG, L. P. & GOW, N. A. 2016. Interactions of fungal pathogens with phagocytes. *Nat Rev Microbiol,* 14**,** 163-76.

FABREGAT, A., JUPE, S., MATTHEWS, L., SIDIROPOULOS, K., GILLESPIE, M., GARAPATI, P., HAW, R., JASSAL, B., KORNINGER, F., MAY, B., MILACIC, M., ROCA, C. D., ROTHFELS, K., SEVILLA, C., SHAMOVSKY, V., SHORSER, S., VARUSAI, T., VITERI, G., WEISER, J., WU, G., STEIN, L., HERMJAKOB, H. & D'EUSTACHIO, P. 2018. The Reactome Pathway Knowledgebase. *Nucleic Acids Res,* 46**,** D649-d655.

FAKHIM, H., VAEZI, A., DANNAOUI, E., CHOWDHARY, A., NASIRY, D., FAELI, L., MEIS, J. F. & BADALI, H. 2018. Comparative virulence of Candida auris with Candida haemulonii, Candida glabrata and Candida albicans in a murine model. *Mycoses,* 61**,** 377-382.

GOW, N. A., NETEA, M. G., MUNRO, C. A., FERWERDA, G., BATES, S., MORA-MONTES, H. M., WALKER, L., JANSEN, T., JACOBS, L., TSONI, V., BROWN, G. D., ODDS, F. C., VAN DER MEER, J. W., BROWN, A. J. & KULLBERG, B. J. 2007. Immune recognition of Candida albicans beta-glucan by dectin-1. *J Infect Dis,* 196**,** 1565-71.

GOW, N. A., VAN DE VEERDONK, F. L., BROWN, A. J. & NETEA, M. G. 2011. Candida albicans morphogenesis and host defence: discriminating invasion from colonization. *Nat Rev Microbiol,* 10**,** 112-22.

GRINGHUIS, S. I., DEN DUNNEN, J., LITJENS, M., VAN DER VLIST, M., WEVERS, B., BRUIJNS, S. C. & GEIJTENBEEK, T. B. 2009. Dectin-1 directs T helper cell differentiation by controlling noncanonical NF-kappaB activation through Raf-1 and Syk. *Nat Immunol,* 10**,** 203-13.

HALL, R. A. & GOW, N. A. 2013a. Mannosylation in Candida albicans: role in cell wall function and immune recognition. *Mol Microbiol,* 90**,** 1147-61.

HALL, R. A. & GOW, N. A. R. 2013b. Mannosylation in Candida albicans: role in cell wall function and immune recognition. *Molecular Microbiology,* 90**,** 1147-1161.

JOHNSON, C. J., DAVIS, J. M., HUTTENLOCHER, A., KERNIEN, J. F. & NETT, J. E. 2018. Emerging Fungal Pathogen Candida auris Evades Neutrophil Attack. *MBio,* 9.

KAMBUROV, A., WIERLING, C., LEHRACH, H. & HERWIG, R. 2009. ConsensusPathDB--a database for integrating human functional interaction networks. *Nucleic Acids Res,* 37**,** D623-8.

KANEHISA, M. & GOTO, S. 2000. KEGG: kyoto encyclopedia of genes and genomes. *Nucleic Acids Res,* 28**,** 27-30.

KATHURIA, S., SINGH, P. K., SHARMA, C., PRAKASH, A., MASIH, A., KUMAR, A., MEIS, J. F. & CHOWDHARY, A. 2015. Multidrug-Resistant Candida auris Misidentified as Candida haemulonii: Characterization by Matrix-Assisted Laser Desorption Ionization-Time of Flight Mass Spectrometry and DNA Sequencing and Its Antifungal Susceptibility Profile Variability by Vitek 2, CLSI Broth Microdilution, and Etest Method. *J Clin Microbiol,* 53**,** 1823-30.

KEPPLER-ROSS, S., DOUGLAS, L., KONOPKA, J. B. & DEAN, N. 2010. Recognition of Yeast by Murine Macrophages Requires Mannan but Not Glucan. *Eukaryotic Cell,* 9**,** 1776-1787.

KLEBANOFF, S. J. 2005. Myeloperoxidase: friend and foe. *J Leukoc Biol,* 77**,** 598-625.

LARKIN, E., HAGER, C., CHANDRA, J., MUKHERJEE, P. K., RETUERTO, M., SALEM, I., LONG, L., ISHAM, N., KOVANDA, L., BORROTO-ESODA, K., WRING, S., ANGULO, D. & GHANNOUM, M. 2017. The Emerging Pathogen Candida auris: Growth Phenotype, Virulence Factors, Activity of Antifungals, and Effect of SCY-078, a Novel Glucan Synthesis Inhibitor, on Growth Morphology and Biofilm Formation. *Antimicrob Agents Chemother,* 61.

LEE, W. G., SHIN, J. H., UH, Y., KANG, M. G., KIM, S. H., PARK, K. H. & JANG, H. C. 2011. First three reported cases of nosocomial fungemia caused by Candida auris. *J Clin Microbiol,* 49**,** 3139-42.

LOCKHART, S. R., ETIENNE, K. A., VALLABHANENI, S., FAROOQI, J., CHOWDHARY, A., GOVENDER, N. P., COLOMBO, A. L., CALVO, B., CUOMO, C. A., DESJARDINS, C. A., BERKOW, E. L., CASTANHEIRA, M., MAGOBO, R. E., JABEEN, K., ASGHAR, R. J., MEIS, J. F., JACKSON, B., CHILLER, T. & LITVINTSEVA, A. P. 2017. Simultaneous Emergence of Multidrug-Resistant Candida auris on 3 Continents Confirmed by Whole-Genome Sequencing and Epidemiological Analyses. *Clin Infect Dis,* 64**,** 134-140.

LOVE, M. I., HUBER, W. & ANDERS, S. 2014. Moderated estimation of fold change and dispersion for RNA-seq data with DESeq2. *Genome Biology,* 15.

MARTIN, M. 2016. Cutadapt Removes Adapter Sequences From High-Throughput Sequencing Reads. *EMBnet.journal,* v. 17.

MCKENZIE, C. G. J., KOSER, U., LEWIS, L. E., BAIN, J. M., MORA-MONTES, H. M., BARKER, R. N., GOW, N. A. R. & ERWIG, L. P. 2010. Contribution of Candida albicans Cell Wall Components to Recognition by and Escape from Murine Macrophages. *Infection and Immunity,* 78**,** 1650-1658.

MEIS, J. F. & CHOWDHARY, A. 2018. Candida auris: a global fungal public health threat. *Lancet Infect Dis*.

MIZUSAWA, M., MILLER, H., GREEN, R., LEE, R., DURANTE, M., PERKINS, R., HEWITT, C., SIMNER, P. J., CARROLL, K. C., HAYDEN, R. T. & ZHANG, S. X. 2017. Can Multidrug-Resistant Candida auris Be Reliably Identified in Clinical Microbiology Laboratories? *J Clin Microbiol,* 55**,** 638-640.

MOHD TAP, R., LIM, T. C., KAMARUDIN, N. A., GINSAPU, S. J., ABD RAZAK, M. F., AHMAD, N. & AMRAN, F. 2018. A Fatal Case of Candida auris and Candida tropicalis Candidemia in Neutropenic Patient. *Mycopathologia,* 183**,** 559-564.

NAVARRO-ARIAS, M. J., HERNANDEZ-CHAVEZ, M. J., GARCIA-CARNERO, L. C., AMEZCUA-HERNANDEZ, D. G., LOZOYA-PEREZ, N. E., ESTRADA-MATA, E., MARTINEZ-DUNCKER, I., FRANCO, B. & MORA-MONTES, H. M. 2019. Differential recognition of Candida tropicalis, Candida guilliermondii, Candida krusei, and Candida auris by human innate immune cells. *Infect Drug Resist,* 12**,** 783-794.

OOSTING, M., BUFFEN, K., CHENG, S. C., VERSCHUEREN, I. C., KOENTGEN, F., VAN DE VEERDONK, F. L., NETEA, M. G. & JOOSTEN, L. A. B. 2015. Borrelia-induced cytokine production is mediated by spleen tyrosine kinase (Syk) but is Dectin-1 and Dectin-2 independent. *Cytokine,* 76**,** 465-472.

PATHIRANA, R. U., FRIEDMAN, J., NORRIS, H. L., SALVATORI, O., MCCALL, A. D., KAY, J. & EDGERTON, M. 2018. Fluconazole-Resistant Candida auris Is Susceptible to Salivary Histatin 5 Killing and to Intrinsic Host Defenses. *Antimicrob Agents Chemother,* 62.

RICHARDSON, J. P. & MOYES, D. L. 2015. Adaptive immune responses to Candida albicans infection. *Virulence,* 6**,** 327-37.

RUDRAMURTHY, S. M., CHAKRABARTI, A., PAUL, R. A., SOOD, P., KAUR, H., CAPOOR, M. R., KINDO, A. J., MARAK, R. S. K., ARORA, A., SARDANA, R., DAS, S., CHHINA, D., PATERL, A., XESS, I., TARAI, B., SINGH, P. & GHOSH, A. 2017. Candida auris candidaemia in Indian ICUs: analysis of risk factors. *Journal of Antimicrobial Chemotherapy,* 72**,** 1794-1801.

RUIZ-GAITAN, A., MORET, A. M., TASIAS-PITARCH, M., ALEIXANDRE-LOPEZ, A. I., MARTINEZ-MOREL, H., CALABUIG, E., SALAVERT-LLETI, M., RAMIREZ, P., LOPEZ-HONTANGAS, J. L., HAGEN, F., MEIS, J. F., MOLLAR-MASERES, J. & PEMAN, J. 2018. An outbreak due to Candida auris with prolonged colonisation and candidaemia in a tertiary care European hospital. *Mycoses,* 61**,** 498-505.

SCHELENZ, S., HAGEN, F., RHODES, J. L., ABDOLRASOULI, A., CHOWDHARY, A., HALL, A., RYAN, L., SHACKLETON, J., TRIMLETT, R., MEIS, J. F., ARMSTRONG-JAMES, D. & FISHER, M. C. 2016. First hospital outbreak of the globally emerging Candida auris in a European hospital. *Antimicrob Resist Infect Control,* 5**,** 35.

URBAN, C. F. & NETT, J. E. 2019. Neutrophil extracellular traps in fungal infection. *Semin Cell Dev Biol,* 89**,** 47-57.

URBAN, C. F., REICHARD, U., BRINKMANN, V. & ZYCHLINSKY, A. 2006. Neutrophil extracellular traps capture and kill Candida albicans yeast and hyphal forms. *Cell Microbiol,* 8**,** 668-76.

VALLABHANENI, S., KALLEN, A., TSAY, S., CHOW, N., WELSH, R., KERINS, J., KEMBLE, S. K., PACILLI, M., BLACK, S. R., LANDON, E., RIDGWAY, J., PALMORE, T. N., ZELZANY, A., ADAMS, E. H., QUINN, M., CHATURVEDI, S., GREENKO, J., FERNANDEZ, R., SOUTHWICK, K., FURUYA, E. Y., CALFEE, D. P., HAMULA, C., PATEL, G., BARRETT, P., LAFARO, P., BERKOW, E. L., MOULTON-MEISSNER, H., NOBLE-WANG, J., FAGAN, R. P., JACKSON, B. R., LOCKHART, S. R., LITVINTSEVA, A. P. & CHILLER, T. M. 2017. Investigation of the First Seven Reported Cases of Candida auris, a Globally Emerging Invasive, Multidrug-Resistant Fungus-United States, May 2013-August 2016. *Am J Transplant,* 17**,** 296-299.

WELSH, R. M., BENTZ, M. L., SHAMS, A., HOUSTON, H., LYONS, A., ROSE, L. J. & LITVINTSEVA, A. P. 2017. Survival, Persistence, and Isolation of the Emerging Multidrug-Resistant Pathogenic Yeast Candida auris on a Plastic Health Care Surface. *J Clin Microbiol,* 55**,** 2996-3005.

ZHU, A., IBRAHIM, J. G. & LOVE, M. I. 2018. Heavy-tailed prior distributions for sequence count data: removing the noise and preserving large differences. *Bioinformatics*.

MAIN FIGURE TITLES AND LEGENDS

Figure 1. Comparative transcriptomic analysis of the host-response upon exposure to live *C. albicans* and *C. auris* and its *in vitro* validation.

Venn diagram representing the number of DEG of both *Candida* species and their relative overlap, reveals substantial overlap between the *C. albicans* and *C. auris* live induced host-response at 24 hours. DEG were subjected to a pathway enrichment analysis, in turn revealing the top 15 *Candida* intrinsic (overlapping DEG, middle panel) and species specific (DEG unique for *C. albicans*, left panel; DEG unique for *C. auris*, right panel) pathways. Enrichment determined using Consensus PathDB, including pathways as defined by KEGG (red) and Reactome (pink), considering a q-value < 0.01 significant. Size of the geometric points indicates the amount of DEG in relation to the pathways' size.

Figure 2. *C. auris* induces a stronger host immune response than *C. albicans* in PBMCs through heat-sensitive component in its cell wall.

(A-B) PBMC production of cytokines TNF-α, IL-6, IL-1β after stimulation without (RPMI; negative control) or with live (A) or heat inactivated (B) *C. albicans* and *C. auris* for 24 hours. Cytokine levels in the supernatant of exposed PBMCs were considered a measure of production.

(C) The BMDM phagocytic capacity of Thimerosal-fixed *C. albicans* or *C. auris* conidia strains in a 3-hour period. BMDM engulfment, depicted as the percentage of macrophages having phagocytosed at least one fungal cell (left). Phagocytic index, considered the number of fungal cells engulfed per 100 macrophages (right).

(D) Distribution of phagocytosed Thimerosal-fixed fungal cells per macrophage in a period of 3 hours.

(E) Killing capacity of live *C. albicans* and *C. auris*, depicted as the percentage of lysed macrophages (BMDM) after 3 hours of exposure. Yeast:Macrophage ratio (MOI) was 3:1.

Graphs represent mean ± SEM, n = 6 – 12, pooled from two to four independent experiments. * $p < 0.05$, *** $p < 0.001$, Wilcoxon signed-rank test (A-B), Mann-Whitney U test (E).

Figure 3. Mannans are fundamental for orchestrating the *C. auris* induced late host response.

(A) Split venn diagrams indicating the number of DEG upon *C. albicans* live stimulation on the left, with its respective overlap between exposure to the purified cell-wall components β-glucan and mannan, and on the right DEG upon *C. auris* live stimulation, with respective overlap. Left split venn diagram visualizes the early, 4-hour response, and the right split venn diagram reflects the late, 24-hour response.

(B) Heatmap displaying the Log_2 fold change (color scale) of the top 50 DEG of *C. albicans* live, for both *Candida* species and their cell-wall components, β-glucan and mannan, at 4 (left panel) and 24 hours (right panel).

Figure 4. Reduced β-glucan surface exposition of *C. auris* and decreased capacity to induce cytokine production compared to *C. albicans*.

(A) Flow cytometry plot demonstrating *C. auris* strains are slightly smaller than *C. albicans*.

(B) Flow cytometry based comparison of cell wall components of *C. albicans* and *C. auris* strains. Mean fluorescent intensity (MFI) of fungal cells stained for Fc-Dectin-1, a marker for β-glucan, and ConA, a marker for mannans.

(C-D) PBMC production of cytokines TNF-α, IL-1β, IL-6 and IL-1RA after 24-hour stimulation without (RPMI; negative control) or with purified β-glucans (C) or mannans (D) from *C. albicans* and various *C. auris* strains in the presence of 10% human serum. Statistical testing was performed on cytokine levels for mannans or β-glucans from each *C. auris* strain in comparison to *C. albicans* SC5314.

(E) Molecular structures of mannans from both *Candida* species.

(F) PBMC production of IL-1β after 24-hour stimulation without (RPMI; negative control) or with Pam3cys and/or purified β-glucans from different *C. auris* and *C. albicans* strains in the presence of 10% human serum.

(G) PBMC production of IL-1β after 24-hour stimulation without (RPMI; negative control) or with purified mannans from *C. albicans* and various *C. auris* strains in the presence of 10% heat-inactivated human serum.

Graphs represent mean ± SEM, n = 6 – 12, pooled from two to four independent experiments. * $p < 0.05$, *** $p < 0.001$, 1-way ANOVA (B), Wilcoxon signed-rank test (C-G).

Figure 5. PRR and signaling pathways involved in the *C. auris* induced cytokine production.

(A) PBMC production of cytokines IL-6 and IL-1β after 24-hour stimulation without (RPMI; negative control) or with live or heat-killed *C. albicans* and *C. auris*, subjected to RPMI or a 1-hour pre-incubation with the PI3K/Akt inhibitor wortmannin.

(B) PBMC production of cytokines IL-6 and IL-1β after 24-hour stimulation without (RPMI; negative control) or with PFA-killed *C. albicans* and *C. auris*, subjected to RPMI or a 1-hour pre-incubation with the Syk inhibitor R406 or Raf-1 inhibitor GW5074.

(C) PBMC production of cytokines IL-6 and IL-1β after 24-hour stimulation without (RPMI; negative control) or with live *C. albicans* and *C. auris*, subjected to a 1-hour pre-incubation with IgG2b, Goat IgG and IgG1 control isotype antibodies, or DC-SIGN, Dectin-1, Mincle, MMR, CR3 and Dectin-2 blocking antibodies. Cytokine levels were compared between the neutralizing antibodies and the correspondent isotype controls.

(D) PBMC production of cytokines IFN-γ, IL-17, IL-22 after 7 days of stimulation without (RPMI; negative control) or with PFA killed *C. albicans* and *C. auris*, subjected to a 1-hour pre-incubation with IgG2b and Goat IgG control isotype antibodies, or DC-SIGN, Mincle, MMR and CR3 blocking antibodies. Cytokine levels were compared between the neutralizing antibodies and the correspondent isotype controls.

(E) PBMC production of cytokines IL-17 and IL-22 after 7 days of stimulation without (RPMI; negative control) or with heat-killed *C. albicans* and *C. auris*, subjected to RPMI or a 1-hour pre-incubation with Syk, Raf-1 or Akt inhibitors.

Graphs represent mean ± SEM, n = 6 – 12, pooled from two to four independent experiments. * $p < 0.05$, *** $p < 0.001$, Wilcoxon signed-rank test.

Figure 6. *C. auris* is less virulent than *C. albicans* in an experimental model of murine disseminated candidiasis.

(A) Survival curve of immunocompetent mice i.v. challenged with *C. albicans* or *C. auris*.

(B) Fungal burden of immunocompetent mice i.v. challenged with *C. albicans* or *C. auris* in the liver and kidney at 3 (top) and 7 (bottom) days post injection.

Mice were i.v. injected with $1x10^7$ CFU of the respective *Candida* strain and monitored daily. Graphs represent mean ± SEM, n = 10 - 11, pooled from at least two independent experiments. * $p < 0.05$, *** $p < 0.001$, Log-rank test (A), Mann-Whitney U test (B).

STAR METHODS

Key Resources Table

REAGENT or RESOURCE	SOURCE	IDENTIFIER
Antibodies		
DC-SIGN Monoclonal Antibody (clone 120507)	Fisher Scientific	MA1-25615
Human Dectin-1/CLEC7A Allophycocyanin Mab (Clone 259931)	Bio-Techne/R&D	MAB1859
Anti-hMincle-IgG	Invivogen	mabg-hmcl
Mouse IgG2B Isotype Control	Bio-Techne/R&D	MAB004
Human Dectin-2/CLEC6A Antibody	Bio-Techne/R&D	MAB3114
IgG1 Isotype Control	Bio-Techne/R&D	MAB002
Human MMR/CD206 Antibody	Bio-Techne/R&D	AF2534
anti-hIntegrin beta2 - hIntegrin b2 Affinity Purified Goat IgG	Bio-Techne/R&D	AF1730
anti-human IgG AlexaFluor 488 conjugate	Life Technologies	
Concanavalin A-Texas Red conjugate	Life Technologies	
Fc-Dectin-1	Gift from Gordon Brown	
Fungal Strains		
C. albicans	ATCC	(ATCC MYA-3573) UC820
C. albicans	Clinical blood isolate	CWZ 10061110
C. auris (Clade II)	J. Meis	KCTC17810 (Clade II)

C. auris (Clade I)	A. Chowdhary	CWZ 10051894 (Clade I)
C. auris (Clade I)	A. Chowdhary	CWZ 10051896 (Clade I)
Biological Samples		
Chemicals, Peptides, and Recombinant Proteins		
Luminol	Sigma-Aldrich	A8511-5G
Zymosan (from S. cerevisiae)	Sigma-Aldrich	Z4250-1G
Pam3Cys	EMC Microcollections	L2000
Syk inhibitor	Merck Chemicals	574711-5MG
Wortmannin PI3K inhibitor	Sas-InvivoGen	tlrl-wtm
Raf-1 inhibitor (GW5074)	Sigma-Aldrich	6416
Ficoll-Paque	GE Healthcare	17-1440-03
Roswell Park Memorial Institute medium (RPMI)	Invitrogen	22406031
Gentamycin	Thermo Fisher Scientific	15750060
Pyruvate	Thermo Fisher Scientific	11360070
C. auris mannans 1	David Williams	KCTC17810 (Clade II)
C. auris mannans 2	David Williams	CWZ 10031160 (2012) (Clade I)
C. auris mannans 3	David Williams	CWZ 10031163 (2012) (Clade I)
C. auris mannans 4	David Williams	CWZ 10051256 (2013) (Clade I)
C. auris mannans 5	David Williams	CWZ 10051263 (2013) (Clade I)
C. auris mannans 6	David Williams	CWZ 10051522 (2014) (Clade IV)
C. auris mannans 7	David Williams	CWZ 10051244 (2014) (Clade I)
C. auris mannans 8	David Williams	CWZ 10051252 (2014) (Clade I)
C. auris β-glucans 1	David Williams	KCTC17810(Clade II)
C. auris β-glucans 2	David Williams	CWZ 10031160 (2012) (Clade I)
C. auris β glucans 3	David Williams	CWZ 10031163 (2012) (Clade I)
C. auris β -glucans 4	David Williams	CWZ 10051256 (2013) (Clade I)
C. auris β glucans 5	David Williams	CWZ10051263 (2013) (Clade I)
C. auris β glucans 6	David Williams	CWZ10051522 (2014) (Clade IV)
C. auris β glucans 7	David Williams	CWZ 10051244 (2014) (Clade I)
C. auris β glucans 8	David Williams	CWZ 10051252 (2014) (Clade I)
Critical Commercial Assays		
Human IL-1b ELISA	R&D Systems	DY201

Human TNFa ELISA	R&D Systems	DY210
Human IL-17 ELISA	R&D Systems	D1700
Human IL-22 ELISA	R&D Systems	D2200
Human IL-6 ELISA	R&D Systems	DY206
Human IL-8 ELISA	Sanquin	M1918
Human IL-10 ELISA	R&D Systems	D1000B
Human IFNg ELISA	Sanquin	M1933
Lactate Fluorometric Assay Kit	Biovision	K607
RNeasy mini Kit	Qiagen	#74104
RNAse-Free DNAse set	Qiagen	#79254
Qubit RNA and DNA HS assay	Thermo Fisher Scientific	#Q32852, #Q32854
RNA and DNA HS ScreenTape	Agilent	#5067-5576, #5067-5582
QuantSeq 3'mRNA-Seq Library prep kit-FWD	Lexogen	015.96
Deposited Data		
Experimental Models: Cell Lines		
Experimental Models: Organisms/Strains		
C57BL/6J mice	Hellenic Institute Pasteur, Athens, Greece	EL 25 BioBr 011
Oligonucleotides		
Recombinant DNA		
Software and Algorithms		
GraphPad Prism	Graphpad Software	https://www.graphpad.com
R programming language	R Development Core Team, 2015.	https://www.R-project.org/
Low quality filtering and adaptor trimming: Trim Galore! v0.4.4_dev Cutadapt v1.18 FastQC v0.11.5	 Babraham Bioinformatics Martin et al., 2011 Babraham Bioinformatics	https://www.bioinformatics.babraham.ac.uk/projects/trim_galore/ https://github.com/marcelm/cutadapt https://www.bioinformatics.babraham.ac.uk/projects/fastqc/
Mapping to human reference genome (GRCh38.95, Ensembl): STAR v2.6.0a	Dobin et al., 2012	https://github.com/alexdobin/STAR

Read counting: HTSeq-count tool v0.11.0	Anders et al., 2015	http://www-huber.embl.de/users/anders/HTSeq/doc/overview.html
Differential gene expression analysis: DESeq2 v1.22.0	Love et al., 2014	https://github.com/mikelove/DESeq2
LogFold Shrinkage with apeglm	Zhu et al., 2018	https://github.com/mikelove/DESeq2
Pathway enrichment analysis: Consensus Path DB	Kamburov et al., 2009	http://consensuspathdb.org
Other		

CONTACT FOR REAGENT AND RESOURCE SHARING

Further information and requests for resources and reagents should be directed to and will be fulfilled by the Lead Contact, Mihai Netea at the Radboud University Medical Center, Nijmegen, the Netherlands (mihai.netea@radboudumc.nl).

EXPERIMENTAL MODEL AND SUBJECT DETAILS

Ethics statement for ex vivo human PBMC stimulations

Inclusion of healthy controls was approved by the local institutional review board (CMO region Arnhem-Nijmegen, #2299 2010/104) and conducted according to the principles of the International Conference on Harmonization–Good Clinical Practice guidelines. Buffy coats from healthy donors were obtained after written informed consent (Sanquin blood bank, Nijmegen, the Netherlands).

Ethics statement for *in vivo* mice studies

Mouse studies were conducted at the Center of Animal Use for Medical/Scientific Purposes of the ATTIKON University General Hospital. The study was approved by the Athens Venerinaty Service following local Ethics approval (approval 97/2017).

METHOD DETAILS

PBMCs isolation and stimulation

Venous blood from the antecubital vein of healthy volunteers was drawn in EDTA tubes after obtaining written informed consent. PBMC isolation was performed as previously described (Oosting et al., 2015). Briefly, the PBMC fraction was obtained using density centrifugation in Ficoll-Paque (Pharmacia Biotech). Cells were then washed twice in PBS and re-suspended in RPMI medium (Invitrogen) supplemented with gentamicin 10 mg/mL, L-glutamine 10 mM and pyruvate 10 mM. Afterwards, PBMCs were counted and re-suspended in a concentration of $5x10^6$ cells /mL. $5x10^5$ PBMCs were added in 100 µL to round-bottom 96-well plates (Greiner) and incubated with 50 µL of stimulus (RPMI, live, paraformaldehyde (PFA) or heat killed *Candida albicans* yeast $1x10^6$ /mL or *Candida auris* $1x10^6$ mL; 100 µg/mL purified *C. albicans* or *C. auris* mannan; 10 µg/mL purified *C. albicans* or *C. auris* β-glucan) and 50 µL of eventual inhibitor or medium with or without 10% human serum. Serum was either complement active, if not otherwise indicated, or heat inactivated by incubation for 30 minutes at 56°C in a water bath according to a commonly used protocol. After 1 hour of pre-incubation with inhibitor or medium, stimuli or medium was added. In detail, for receptor blockade experiments, before stimulation with *C. albicans* or *C. auris*, PBMCs were pre-incubated for 1 hour with 5 µg/mL anti-DC SIGN antibody 10 µg/mL, anti-Dectin-1, 10 µg anti Mincle and 10 µg/mL control IgG2b; 10 µg/mL anti-Dectin-2 antibody and 10 µg/mL of its control IgG1]); 10 µg/mL anti-CR3 antibody and control IgG (R&D), 10 µg/mL MR-blocking antibody and 10 µg/mL Goat IgG isotype control. After 1 hour, cells were stimulated with 10^6 heat-killed *C. albicans* and *C. auris*. For the intracellular pathways blockade experiment 50 nM Syk inhibitor 10 or 100 nM wortmannin, 1 µM Raf-inhibitor or the same concentration of vehicle (DMSO) has been used. Concentrations of inhibitors were selected as being the highest non-cytotoxic concentrations. All supernatants were stored at -20°C until analyzed.

Cytokine and lactate measurements

All cytokine levels were measured in the cell culture supernatants using commercially available ELISA assays according to the protocol supplied by the manufacturer. IL-1β, TNFα, IL-6, IL-1Ra and IL-10 were measured after 24 hours, and IL-17, IL-22 and IFN-γ were measured after 7 days of stimulation. Lactate was measured by a Lactate Fluorometric Assay Kit (Biovision, CA, USA).

Candida strains

C. auris strains from three clades have been used (Clade I, South Asia; Clade II, East Asia; Clade IV, South America). Unless otherwise indicated, experiments were performed using *C. albicans* CWZ10061110, *C. albicans* UC820 (ATCC MYA-3573), *C. auris* KCTC17810 reference, *C. auris*

CWZ10051894 and *C. auris* CWZ10051896. Stimulations were performed using either live, heat-killed (12 hours at 56°C) or 4% PFA-killed microorganisms.

Isolation and purification of *C. auris* and *C. albicans* cell wall components

For isolation of cell wall β-glucans and mannans, *C. auris* strains were cultivated in 25 mL of YPD (1% yeast extract, 2% dextrose, 2% peptone) for 48 hours at 30˚C. The cells were harvested by centrifugation at 5,000x g for 5 minutes and pellet washed once with dH_2O. The washed cell pellets were then frozen at -20˚C overnight. Prior to extracting the cell wall β-glucans and mannans, the cell pellets were subjected to repeated freeze-thaw cycles (3X) to lyse the cells. Cell pellets were then extracted with a base/acid isolation approach. The supernatant contained the water soluble mannans, which were dialyzed (2000 MWCO) to remove salts and lyophilized to dryness. Glucans are water insoluble and were harvested by centrifugation and washing in dH_2O prior to lyophilization. The structure and purity of the β-glucans and mannans was determined by solution, high field one and two-dimensional Nuclear Magnetic Resonance Spectroscopy (1 and 2-D NMR).

RNA purification

PBMCs from three healthy donors, with a concentration of 5 x 10^6 cells / mL, were stimulated with *C. albicans*, *C. auris* and purified cell wall components β-glucan and mannans isolated from both *Candida* species as described above. PBMCs were cultured in the presence of 10% human pooled serum. At 4 and 24 hours cells were lysed with RLT buffer. Prior to subjection to the RNeasy Mini Kit (Qiagen), lysates were homogenized using a 1 mL syringe with a 0.8 x 15 mm needle. RNA was subsequently extracted following manufacturers' protocol, including an on-column DNAse digestion using the RNAse-Free DNAse set (Qiagen). Quantification and quality assessment of extracted RNA was performed using the Qubit RNA HS assay (Thermo Fisher Scientific) and Agilent 2200 TapeStation (RNA HS Screentape, Agilent), respectively. Majority of samples subjected to quality assessment revealed a RNA integrity number (RIN^e) of ≥ 8.

QuantSeq 3' mRNA sequencing

Libraries were generated from the extracted RNA using the QuantSeq 3' mRNA-Seq Library Prep Kit-FWD from Lexogen (Lexogen) in accordance to the manufacturers' protocol. Three separate preparations were performed, split by PBMC donor, in turn limiting the number of samples to 14 to 18 samples per prep. RNA input was normalized to 100 ng for donor A, and to 250 ng for donors B and C. An aliquot (1:10) of double stranded cDNA libraries was used for quantitative PCR, in turn indicating

17 – 18 cycles as optimal for endpoint PCR (17- donor B; 18 - donors A, C). Accurate quantification and assessment of quality of the generated libraries was performed using Qubit dsDNA HS assay (Thermo Fisher Scientific) and Agilent 2200 TapeStation (HS-D1000 ScreenTape, Agilent). The cDNA concentration and average fragment size were used to determine the molar concentration of the individual libraries. Consequently, libraries were pooled equimolar to 100 fmol. After a final dilution of the pool to a concentration of 4 nM, the libraries were sequenced on a NextSeq 500 instrument (Illumina), with 75 cycle (i.e. 75bp single-end sequence reads), high output kit with a 1.1 pM final loading concentration.

Differential gene expression analysis

Quality of the acquired sequencing data was controlled using FastQC tool v0.11.5 (Babraham Bioinformatics) and subsequently followed by the removal of adapter sequences and poly(A) tails with Trim Galore! v.0.4.4_dev (Babraham Bioinformatics) and Cutadapt v1.18 (Martin, 2016). On average ~ 6 million reads per individual library were retrieved. Filtered and trimmed reads were mapped to the human reference genome (hg38/GRCh38) using the STAR aligner v2.6.0a (Table S1) (Dobin et al., 2013). Less than 1% of all reads were comprised of overrepresented sequences and were uniquely mapped with a median of 4 million reads (74.1%). After generating gene level count data using the HTSeq-count tool v0.11.0 (Anders et al., 2015), an additional filtering step was performed ensuring the exclusion of several non-coding RNAs, i.e. mtRNA, lincRNA, snRNA, tRNA, miscRNA and snoRNA, in our dataset. Given the absence of sample replicates, PBMC donors were considered biological replicates. Hence, in the differential gene expression analysis using DESeq2 v1.22.0 (Love et al., 2014), including logFold Shrinkage and apeglm (Zhu et al., 2018), the average PBMC donor response to the different stimuli were compared to their control condition, RPMI. Genes with a fold change of ≥2 and a p-adjusted value <0.01 were considered differentially expressed genes (DEG).

Pathway enrichment analysis

In order to distinguish between the responses triggered by both *Candida* species, DEG were compared between species for the analogous stimulations (live, mannan and β-glucan), and corresponding time-points. In turn resulting a group of DEG that overlap between the two species, and DEG that were uniquely attributed to either one of the *Candida* species. Overrepresentation analysis were performed on all groups per stimulation (and time-point) using Consensus PathDB (Kamburov et al., 2009), including pathways as defined by pathway databases Kyoto Encyclopedia of Genes and Genomes

KEGG (Kanehisa and Goto, 2000) and Reactome (Fabregat et al., 2018). Minimum overlap in input was set at 2, together with a p-value cut-off of 0.01. For downstream analysis, pathways were considered enriched with a corrected p-value <0.01 (indicated as 'q-value').

Reactive oxygen species (ROS) assay

The induction of reactive oxygen species (ROS) was measured by oxidation of luminal (5-amino-2,3, dihydro-1,4-phtalazinedione) and determined in an automated LB96V Microlumat plus luminometer (EG & G Berthold, Bald Wilberg, Germany). Briefly, PBMCs (5×10^5 per well) or neutrophils (2.5×10^5) per well were seeded into white 96-well plates and incubated in medium containing either RPMI, Zymosan (100 µg/mL), heat-killed opsonized *C. albicans* or *C. auris* yeast (10^7 CFU/mL). 20 µL of 1 mM Luminol was added to each well in order to start the chemiluminescence reaction. Each measurement was carried out at least in duplicate. Chemiluminescence was determined every 145 seconds at 37°C for 1 hour. Luminescence was expressed as relative light units (RLU) per second. The RLU/sec within the area under the curve (AUC) were plotted against time and analyzed by using Graphpad Prism v.5.0.

Phagocytosis assay

Bone marrow was extracted from femurs and tibias of eight week old male C57BL/6 mice and differentiated for 7 days with RPMI Medium 1640 Glutamax (Gibco) supplemented with 10% heat-inactivated foetal calf serum, 100 U/mL Penicillin/Streptomycin and 15% L929 cell-conditioned medium at 37°C with 5% CO_2. BMDM were added to 8 well u-slide (ibidi) at 0.5 $x10^5$ cells per well to adhere overnight. *C. albicans* and *C. auris* strains were prepared by growing cells for 24 hours in Sabouraud broth at 30°C with 3 washes in PBS, thereafter. Fixed *Candida* were prepared by incubating the Sabouraud-grown yeast overnight at room temperature in 50 Mm Thimerosal (Sigma) with 5 wash steps in PBS, thereafter. Phagocytosis dynamics were determined following the addition of 3:1; yeast: BMDM. Live imaging of macrophage interactions with live or fixed *C. albicans* and *C. auris* were performed using a Nikon Ti Eclipse microscope with objective 20x magnification set to acquire images at 1 minute intervals using Volocity software (PerkinElmer), with thanks to the University of Aberdeen Microscopy Core Facility. Movies generated from 3 hour interactions were analyzed to determine over time the proportion of macrophages phagocytosing yeast (% uptake), the number of yeast phagocytosed per 100 macrophages (phagocytic index), the proportion of macrophage death after 3 hours (macrophage lysis) and the distribution of yeast contained within individual macrophages.

784 Experiments were performed on 3 occasions, with a total of 9 movies generated per condition.
785 Statistical analyses were performed by ANOVA using GraphPad Prism.

786 ## Cell wall staining

787 Fixed *Candida* yeast were stained for exposed cell wall β-glucans using Fc-Dectin-1 (a gift from Gordon
788 Brown, University of Aberdeen) and secondary F(ab')2 anti-human IgG AlexaFluor 488 conjugate (Life
789 Technologies). ConA-Texas Red conjugate (Life Technologies) was used to detect cell wall mannans.
790 Cells were counted and 2.5 x 10^6 yeast were combined with FACS wash (1% bovine serum albumin and
791 5 mM EDTA in PBS) with either Fc-Dectin-1 at 1 µg/mL or ConA at 25 µg/mL. After a 30 min incubation
792 on ice, cells were washed twice in FACS wash, then incubated with secondary F(ab')2 (for Fc-Dectin-1
793 only) on ice for 45 minutes, with a further 2 wash steps. Flow cytometry was performed on an LSR
794 Fortessa cytometer (BD) with thanks to the University of Aberdeen IFCC Core Facility.

795 ## *In vivo* experiments

796 Experiments were conducted in a total of 200 C57Bl6 male mice. Healthy mice were i.v. challenged via
797 the tail vein with 1x10^7 CFU/mouse log-phase inoculum of three different isolates of *C. albicans* and *C.*
798 *auris* following slight ether anesthesia. Survival was recorded for 14 days; three and seven days post
799 challenge mice were sacrificed by the intramuscular injection of ketamine. After a midline incision
800 under aseptic conditions, the entire spleen was removed and segments of the right kidney and of the
801 liver were cut and put into separate sterile containers. Splenocytes were isolated by gentle passage of
802 cells through a 250 nm filter. After counting of viable cells through trypan blue exclusion, cells were
803 incubated at a density of 5x10^6 /mL without/with 5x10^6 CFU/mL of heat-killed *C. albicans* and *C. auris*
804 in 1640 RPMI enriched with 2 mM glutamine and 10% FBS in the presence of 100 U/mL of penicillin G
805 and 0.1 mg/mL of gentamicin. After five days of incubation at 37^0C in 5% CO_2, plates were centrifuged
806 and supernatants were collected for cytokine measurements. Removed kidneys and livers were
807 weighted and homogenized. The number of fungal counts were measured via serial dilutions 1:10 at
808 0.9% saline and expressed as log10 CFU/g.

809 ## Statistical analysis

810 Statistical analysis, except where otherwise indicated, was performed using the GraphPad Prism 5
811 software. All experiments were performed at least in duplicate. Paired or unpaired t-test, or ANOVA

were used to establish statistical significance (see figure legends for details) and differences between groups were considered significant at p-values of <0.05.

SUPPLEMENTAL VIDEO

Video S1. Aside from its ability to duplicate outside the host, *C. auris* is able to multiply within phagosomes, yet at a slower pace. Related to figure 2 and S3. Live video microscopy of macrophages in the presence of *C. auris* 10051893, for a period of 120 minutes.

Video S2. Extensive accumulation of *C. auris* in macrophages. Related to figure 2 and S3. Live video microscopy of macrophages in the presence of *C. auris* 10051895, for a period of 120 minutes, one hour after stimulation.

Video S3. Maintained duplication of *C. auris* after phagocytosis alterates its MOI. Related to figure 2 and S3. Live video microscopy of macrophages in the presence of *C. auris* 10051895, for a period of 120 minutes, one hour after stimulation.

Video S4. *C. albicans*, once phagocytosed, is able to lyse macrophages. Related to figure 2 and S3. Live video microscopy of macrophages in the presence of *C. albicans* 10061110, for a period of 120 minutes, one hour after stimulation.

SUPPLEMENTARY FIGURES

Figure S1. Transcriptomic profiling PBMCs stimulated with live *C. albicans* or *C. auris* and respective cell wall components β-glucans and mannans for 4 and 24 hours.

(A) PCA of normalized data displaying the variance of conditions to each stimulus (color) and time-point (shape).

(B) PCA displaying the variance at 4 (left panel) and 24-hours (right panel) for each stimulus (color) and donor (shape).

(C) Pathway enrichment plot displaying the top 20 enriched pathways for both *C. albicans* live and *C. auris* live (color) at 24 hours. Enrichment determined using Consensus PathDB, including pathways as defined by KEGG and Reactome (shape), considering a q-value < 0.01 significant. Size of the geometric points indicates the amount of DEG in relation to the pathways' size.

Figure S2. Comparative innate host immune response between *C. albicans* and *C. auris*.

(A) Log_2Fold Change of *IL-6*, *IL-1β* and *IL-1RN* (encoding for IL-1Ra) gene expression in PBMCs stimulated for 24 hours with *C. albicans* and *C. auris*, and their respective purified β-glucans.

(B) Log_2Fold Change of *IL-6*, *IL-1β* and *IL-1RN* (encoding for IL-1Ra) gene expression in PBMCs stimulated for 24 hours with *C. albicans* and *C. auris*, and their respective purified mannans.

(C) PBMC production of cytokines IL-1Ra after stimulation without (RPMI; negative control) or with live or heat-killed *C. albicans* and *C. auris* for 24 hours.

(D) PBMC production of cytokines IFN-γ, IL-10, IL-17 and IL-22 after stimulation without (RPMI; negative control) or with heat-killed *C. albicans* and *C. auris* for 7 days.

Graphs represent mean ± SEM, n = 6 – 12, pooled from two to four independent experiments. * $p < 0.05$, *** $p < 0.001$, Wilcoxon signed-rank test.

Figure S3. Phagocytosis dynamics and ROS production of *C. auris* compared to *C. albicans*.

(A) The BMDM phagocytic capacity of live *C. albicans* or *C. auris* conidia strains in a 3-hour period. BMDM engulfment, depicted as the percentage of macrophages having phagocytosed at least one fungal cell (left). Phagocytic index, considered the number of fungal cells engulfed per 100 macrophages (right).

(B) The BMDM phagocytic capacity of live *C. albicans* or *C. auris* conidia strains. 1-hour BMDM engulfment, depicted as the percentage of macrophages having phagocytosed at least one fungal cell (left). 3-hour BMDM phagocytic index, considered the number of fungal cells engulfed per 100 macrophages (right).

(C) Distribution of phagocytosed live fungal cells per macrophage in a period of 3 hours.

(D) 1-hour time-course of ROS production of PBMCs (left) and neutrophils (right) monitored directly after stimulation without (RPMI; negative control) or with Zymosan (positive control), or heat-killed *C. albicans* and *C. auris*, depicted as area of light units (RLU) per second.

(E) Luminol oxidation as measure of ROS production of PBMCs (left) and neutrophils (right) monitored directly after stimulation without (RPMI; negative control) or with Zymosan (positive control), or heat-killed *C. albicans* and *C. auris*, depicted as area under the curve of relative of RLU / second.

Graphs represent mean ± SEM, n = 6 – 12, pooled from two to four independent experiments. * $p < 0.05$, *** $p < 0.001$, 1-way ANOVA (B), Wilcoxon signed-rank test (E).

Figure S4. Comparative innate host immune response between opsonized and non-opsonized *C. albicans* and *C. auris* and respective cell wall components.

(A) PBMC production of cytokines TNF-α, IL-6 and IL-1RA after 24-hour stimulation without (RPMI; negative control) or with purified mannans from *C. albicans* and various *C. auris* strains in the presence of 10% heat-inactivated serum. Statistical testing was performed on cytokine levels for each *C. auris* strain in comparison to *C. albicans* SC5314.

(B-C) PBMC production of cytokines IFN-γ, IL-17 and IL-22 after 7 days of stimulation without (RPMI; negative control) or with purified mannans from *C. albicans* and various *C. auris* strains in the presence of 10% normal serum (B) or 10% heat-inactivated serum (C). Statistical testing was performed on cytokine levels for each *C. auris* strain in comparison to *C. albicans* SC5314.

(D) PBMC production of cytokines TNFα, IL-6 and IL-1Ra after 24-hour stimulation without (RPMI; negative control) or with Pam3cys and/or purified β-glucans from different *C. auris* and *C. albicans* strains in the presence of 10% human serum.

Graphs represent mean ± SEM, n = 6 – 12, pooled from two to four independent experiments. * p < 0.05, *** p < 0.001, Wilcoxon signed-rank test.

Figure S5. The effect of blocking PRR and signaling pathways on the *C. albicans* and *C. auris* induced cytokine production.

(A) PBMC production of cytokines IFN-γ and IL-10 after 48-hour stimulation without (RPMI; negative control) or with heat-killed *C. albicans* and *C. auris*, subjected to RPMI or a 1-hour pre-incubation with Syk, Raf-1 or Akt inhibitors.

(B) PBMC production of cytokines IFN-γ after 7 days of stimulation without (RPMI; negative control) or with heat-killed *C. albicans* and *C. auris*, subjected to RPMI or a 1-hour pre-incubation with Syk, Raf-1 or Akt inhibitors.

(C) PBMC production of cytokines IL-1Ra and TNF-α after 24-hour stimulation without (RPMI; negative control) or with live *C. albicans* and *C. auris*, subjected to a 1-hour pre-incubation with IgG2b, Goat IgG and IgG1 control isotype antibodies, or DC-SIGN, Dectin-1, Mincle, MMR, CR3 and Dectin-2 blocking antibodies. Cytokine levels were compared between the neutralizing antibodies and the correspondent isotype controls.

(D) PBMC production of cytokines IL-1Ra and TNF-α after 24-hour stimulation without (RPMI; negative control) or with live or heat-killed *C. albicans* and *C. auris*, subjected to RPMI or a 1-hour pre-incubation with the PI3K/Akt inhibitor Wortmannin.

(E) PBMC production of cytokines IL-1Ra and TNF-α after 24-hour stimulation without (RPMI; negative control) or with PFA-killed *C. albicans* and *C. auris*, subjected to RPMI or a 1-hour pre-incubation with the Syk inhibitor R406 or Raf-1 inhibitor GW5074.

Graphs represent mean ± SEM, n = 3 – 12, pooled from two to four independent experiments. * p < 0.05, *** p < 0.001, Wilcoxon signed-rank test.

SUPPLEMENTARY TABLES

Table S1. Quality assessment of sequenced libraries. Per donor and sample. subdivided based on species. stimulation and time-point. the overall coverage and uniquely mapped reads of the sequenced libraries are depicted.

Table S2. Significantly enriched pathways of species unique and species overlapping DEG upon live β-glucan and mannan exposure at 4 hours. Enrichment was determined using Consensus PathDB. including pathways as defined by KEGG and Reactome. and were considered enriched with a corrected p-value (q-value) <0.01.

Table S3. Significantly enriched pathways of species unique and species overlapping DEG upon live β-glucan and mannan exposure at 24 hours. Enrichment was determined using Consensus PathDB. including pathways as defined by KEGG and Reactome. and were considered enriched with a corrected p-value (q-value) <0.01.

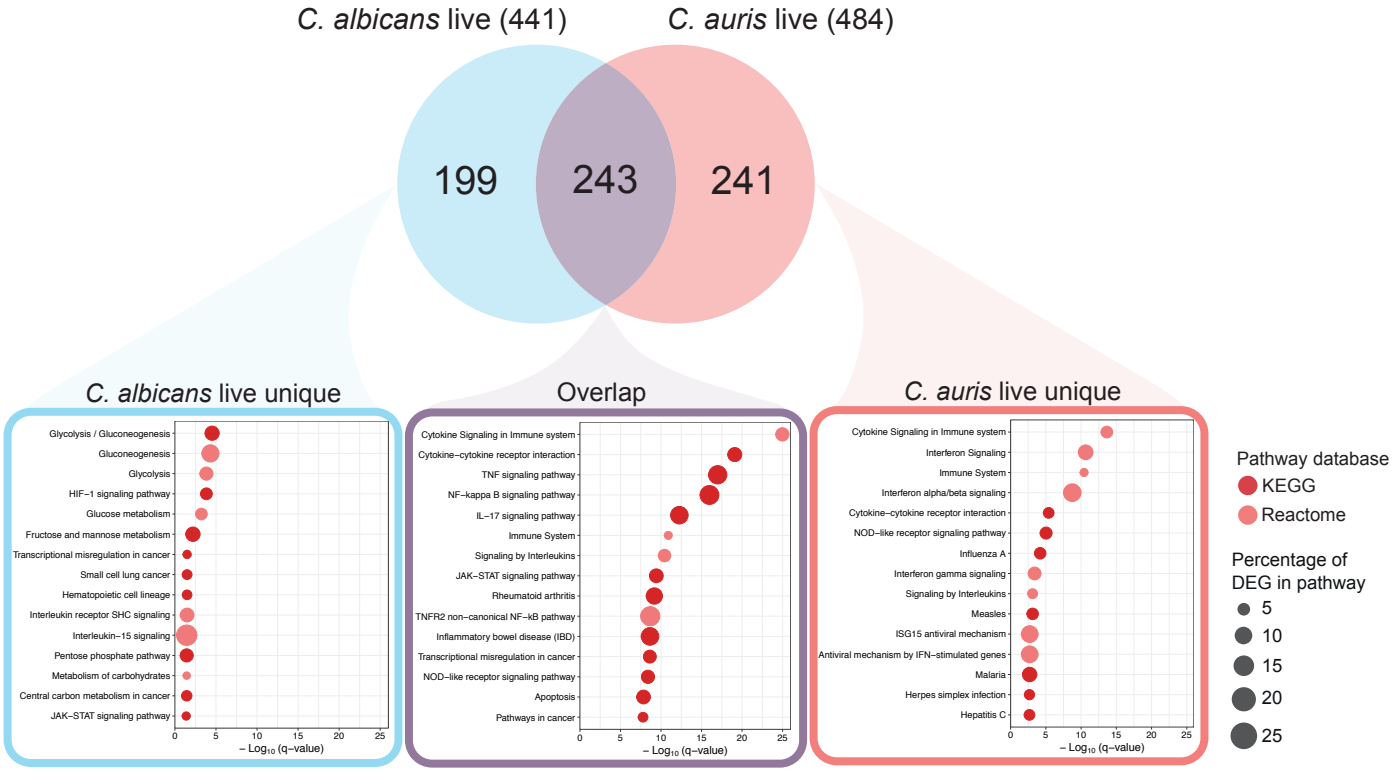
C. albicans live (441)
C. auris live (484)
199
243
241
C. albicans live unique
Glycolysis / Gluconeogenesis
Gluconeogenesis
Glycolysis
HIF−1 signaling pathway
Glucose metabolism
Fructose and mannose metabolism
Transcriptional misregulation in cancer
Small cell lung cancer
Hematopoietic cell lineage
Interleukin receptor SHC signaling
Interleukin−15 signaling
Pentose phosphate pathway
Metabolism of carbohydrates
Central carbon metabolism in cancer
JAK−STAT signaling pathway
0 5 10 15 20 25
− Log10 (q−value)
Overlap
Cytokine Signaling in Immune system
Cytokine−cytokine receptor interaction
TNF signaling pathway
NF−kappa B signaling pathway
IL−17 signaling pathway
Immune System
Signaling by Interleukins
JAK−STAT signaling pathway
Rheumatoid arthritis
TNFR2 non−canonical NF−kB pathway
Inflammatory bowel disease (IBD)
Transcriptional misregulation in cancer
NOD−like receptor signaling pathway
Apoptosis
Pathways in cancer
0 5 10 15 20 25
− Log10 (q−value)
C. auris live unique
Cytokine Signaling in Immune system
Interferon Signaling
Immune System
Interferon alpha/beta signaling
Cytokine−cytokine receptor interaction
NOD−like receptor signaling pathway
Influenza A
Interferon gamma signaling
Signaling by Interleukins
Measles
ISG15 antiviral mechanism
Antiviral mechanism by IFN−stimulated genes
Malaria
Herpes simplex infection
Hepatitis C
0 5 10 15 20 25
− Log10 (q−value)
Pathway database
KEGG
Reactome
Percentage of DEG in pathway
5
10
15
20
25

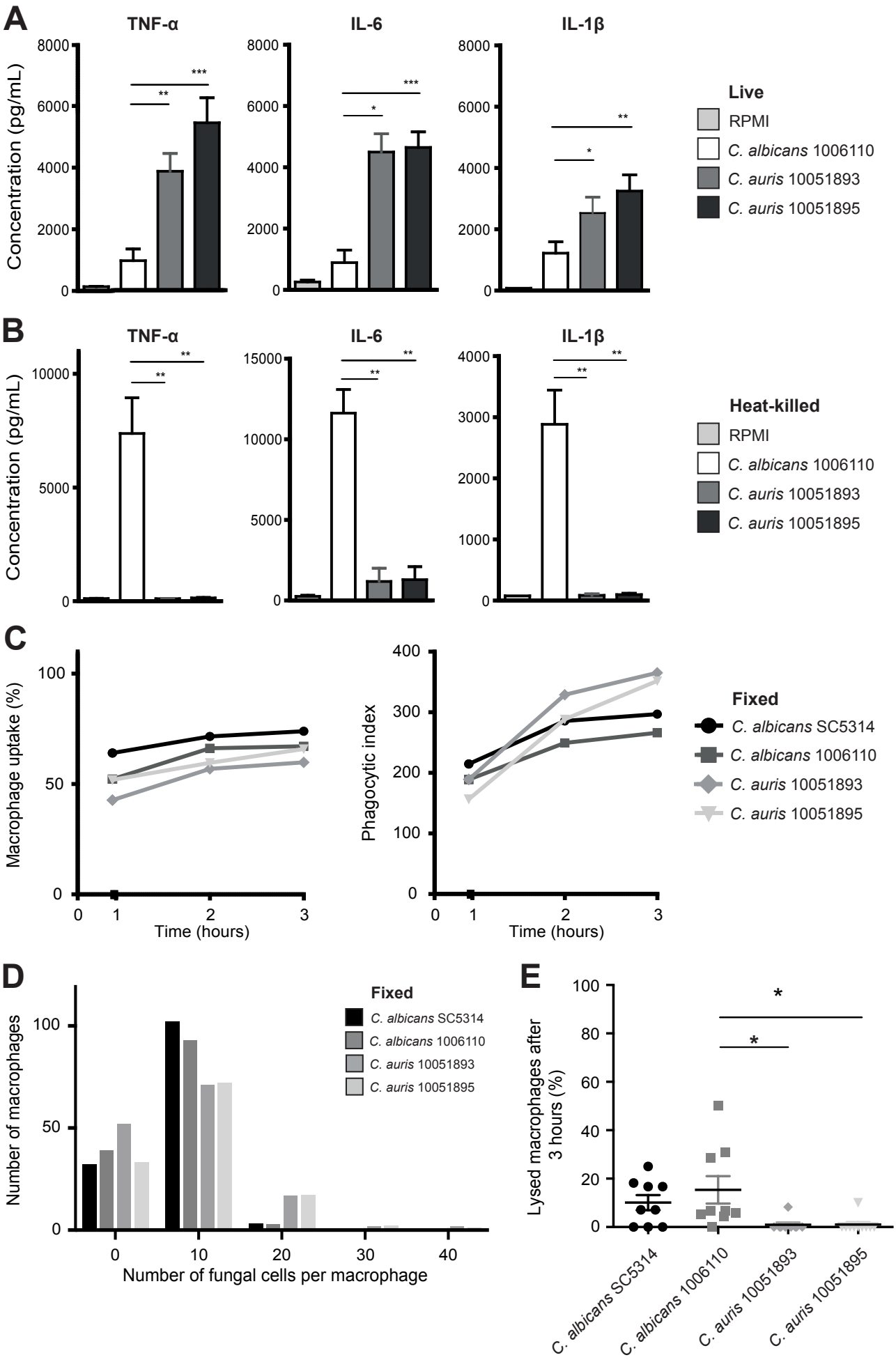
A
TNF-α
IL-6
IL-1β
Concentration (pg/mL)
8000
6000
4000
2000
0
***
**
*
Live
RPMI
C. albicans 1006110
C. auris 10051893
C. auris 10051895
B
TNF-α
IL-6
IL-1β
Concentration (pg/mL)
10000
5000
0
15000
4000
3000
2000
1000
Heat-killed
RPMI
C. albicans 1006110
C. auris 10051893
C. auris 10051895
C
Macrophage uptake (%)
100
50
0
Time (hours)
Phagocytic index
400
300
200
100
Fixed
C. albicans SC5314
C. albicans 1006110
C. auris 10051893
C. auris 10051895
D
Number of macrophages
Number of fungal cells per macrophage
0
10
20
30
40
Fixed
C. albicans SC5314
C. albicans 1006110
C. auris 10051893
C. auris 10051895
E
Lysed macrophages after 3 hours (%)
100
80
60
40
20
0
C. albicans SC5314
C. albicans 1006110
C. auris 10051893
C. auris 10051895

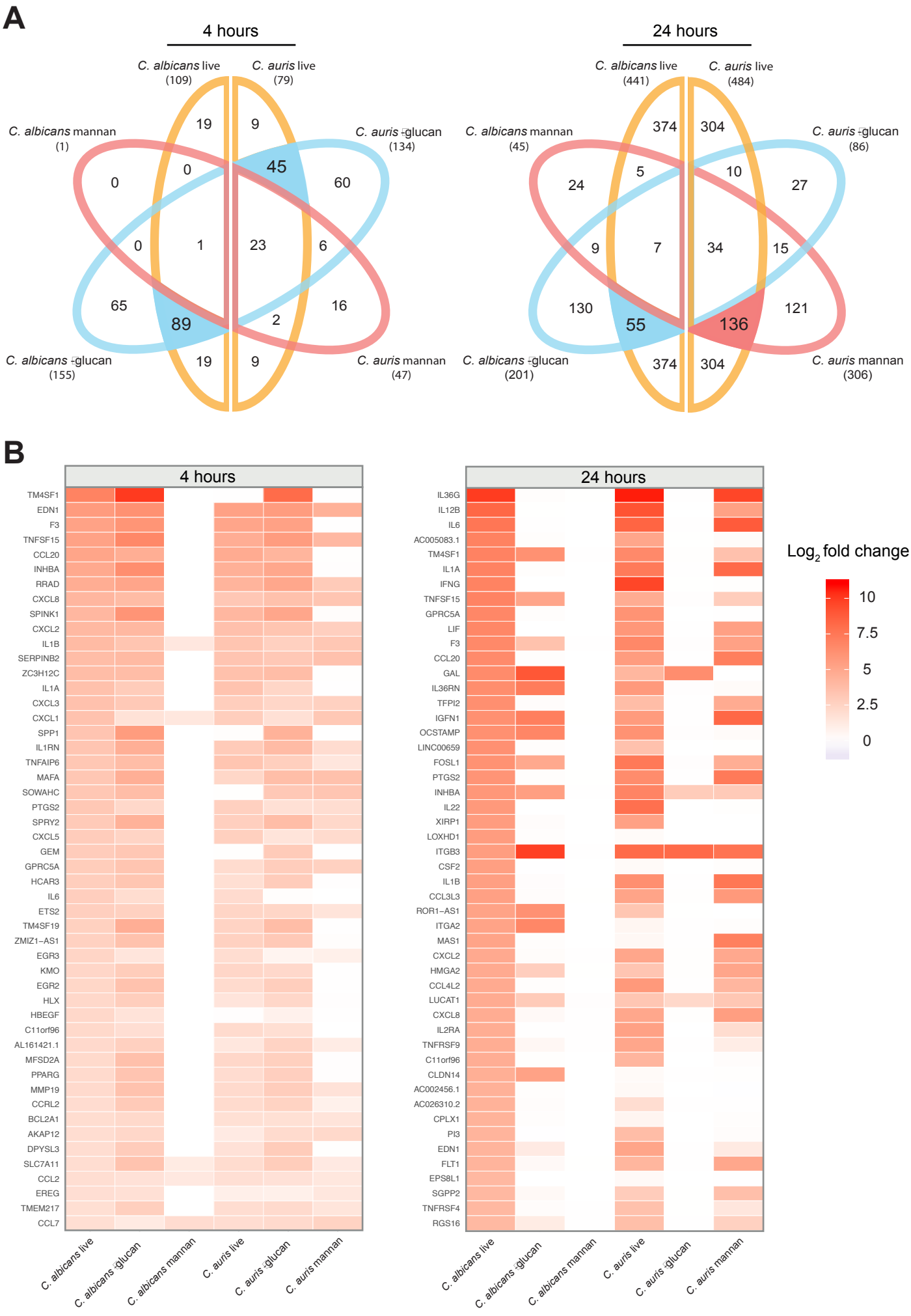
A
4 hours
C. albicans live (109)
C. auris live (79)
C. albicans mannan (1)
C. auris β-glucan (134)
C. albicans β-glucan (155)
C. auris mannan (47)
19
9
0
45
0
60
0
1
23
6
65
89
2
16
19
9
24 hours
C. albicans live (441)
C. auris live (484)
C. albicans mannan (45)
C. auris β-glucan (86)
C. albicans β-glucan (201)
C. auris mannan (306)
374
304
24
5
10
27
9
7
34
15
130
55
136
121
374
304
B
4 hours
TM4SF1
EDN1
F3
TNFSF15
CCL20
INHBA
RRAD
CXCL8
SPINK1
CXCL2
IL1B
SERPINB2
ZC3H12C
IL1A
CXCL3
CXCL1
SPP1
IL1RN
TNFAIP6
MAFA
SOWAHC
PTGS2
SPRY2
CXCL5
GEM
GPRC5A
HCAR3
IL6
ETS2
TM4SF19
ZMIZ1−AS1
EGR3
KMO
EGR2
HLX
HBEGF
C11orf96
AL161421.1
MFSD2A
PPARG
MMP19
CCRL2
BCL2A1
AKAP12
DPYSL3
SLC7A11
CCL2
EREG
TMEM217
CCL7
C. albicans live
C. albicans β-glucan
C. albicans mannan
C. auris live
C. auris β-glucan
C. auris mannan
24 hours
IL36G
IL12B
IL6
AC005083.1
TM4SF1
IL1A
IFNG
TNFSF15
GPRC5A
LIF
F3
CCL20
GAL
IL36RN
TFPI2
IGFN1
OCSTAMP
LINC00659
FOSL1
PTGS2
INHBA
IL22
XIRP1
LOXHD1
ITGB3
CSF2
IL1B
CCL3L3
ROR1−AS1
ITGA2
MAS1
CXCL2
HMGA2
CCL4L2
LUCAT1
CXCL8
IL2RA
TNFRSF9
C11orf96
CLDN14
AC002456.1
AC026310.2
CPLX1
PI3
EDN1
FLT1
EPS8L1
SGPP2
TNFRSF4
RGS16
C. albicans live
C. albicans β-glucan
C. albicans mannan
C. auris live
C. auris β-glucan
C. auris mannan
Log2 fold change
10
7.5
5
2.5
0

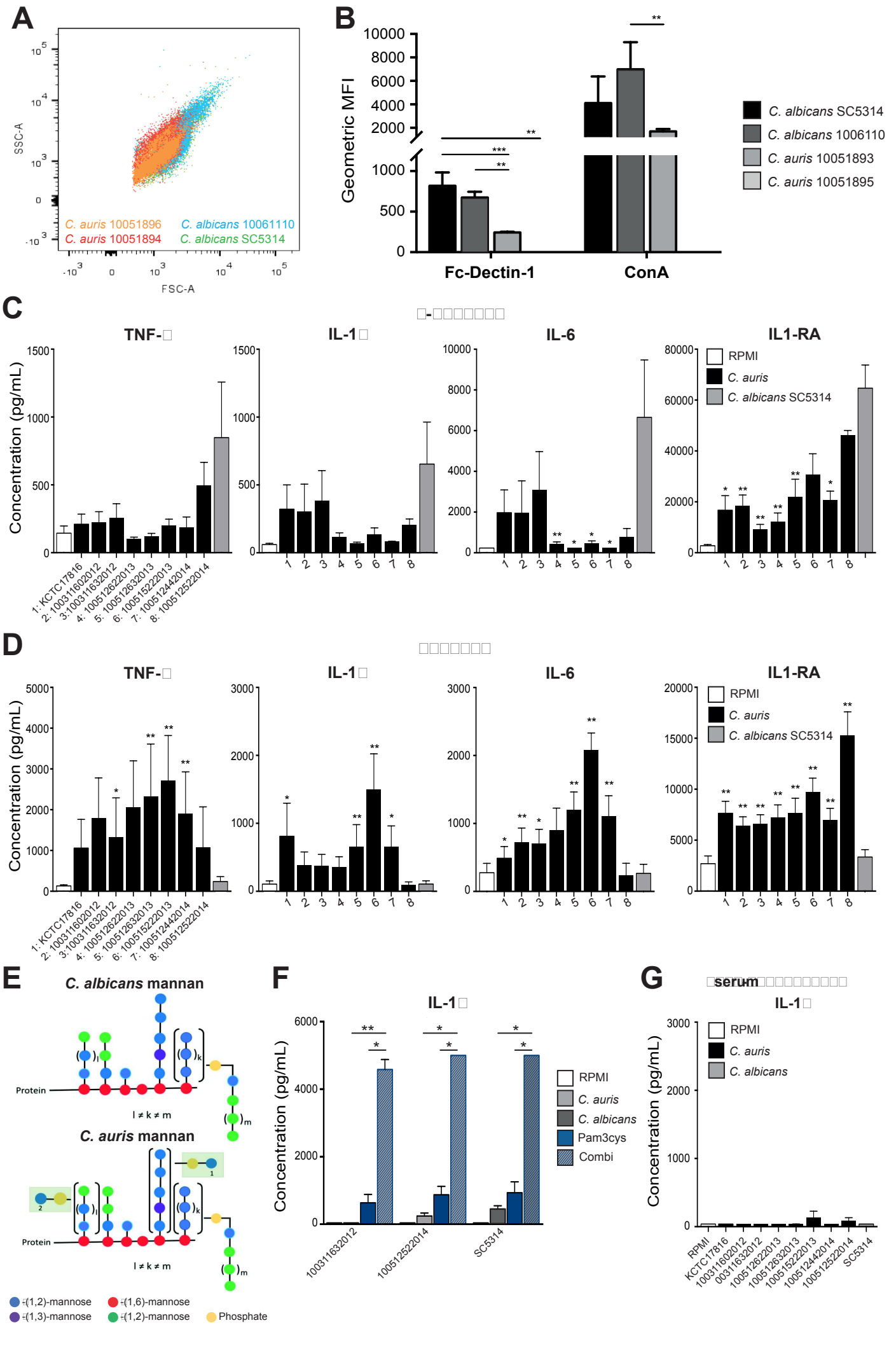
A
SSC-A
FSC-A
C. auris 10051896
C. albicans 10061110
C. auris 10051894
C. albicans SC5314
B
Geometric MFI
Fc-Dectin-1
ConA
C. albicans SC5314
C. albicans 1006110
C. auris 10051893
C. auris 10051895
C
TNF-□
IL-1□
IL-6
IL1-RA
Concentration (pg/mL)
RPMI
C. auris
C. albicans SC5314
1: KCTC17816
2: 100311602012
3:100311632012
4: 100512622013
5: 100512632013
6: 100515222013
7: 100512442014
8: 100512522014
D
TNF-□
IL-1□
IL-6
IL1-RA
Concentration (pg/mL)
RPMI
C. auris
C. albicans SC5314
E
C. albicans mannan
C. auris mannan
Protein
l ≠ k ≠ m
α-(1,2)-mannose
α-(1,6)-mannose
β-(1,3)-mannose
β-(1,2)-mannose
Phosphate
F
IL-1□
Concentration (pg/mL)
RPMI
C. auris
C. albicans
Pam3cys
Combi
100311632012
100512522014
SC5314
G
serum
IL-1□
Concentration (pg/mL)
RPMI
C. auris
C. albicans
RPMI
KCTC17816
100311602012
100311632012
100512622013
100512632013
100515222013
100512442014
100512522014
SC5314

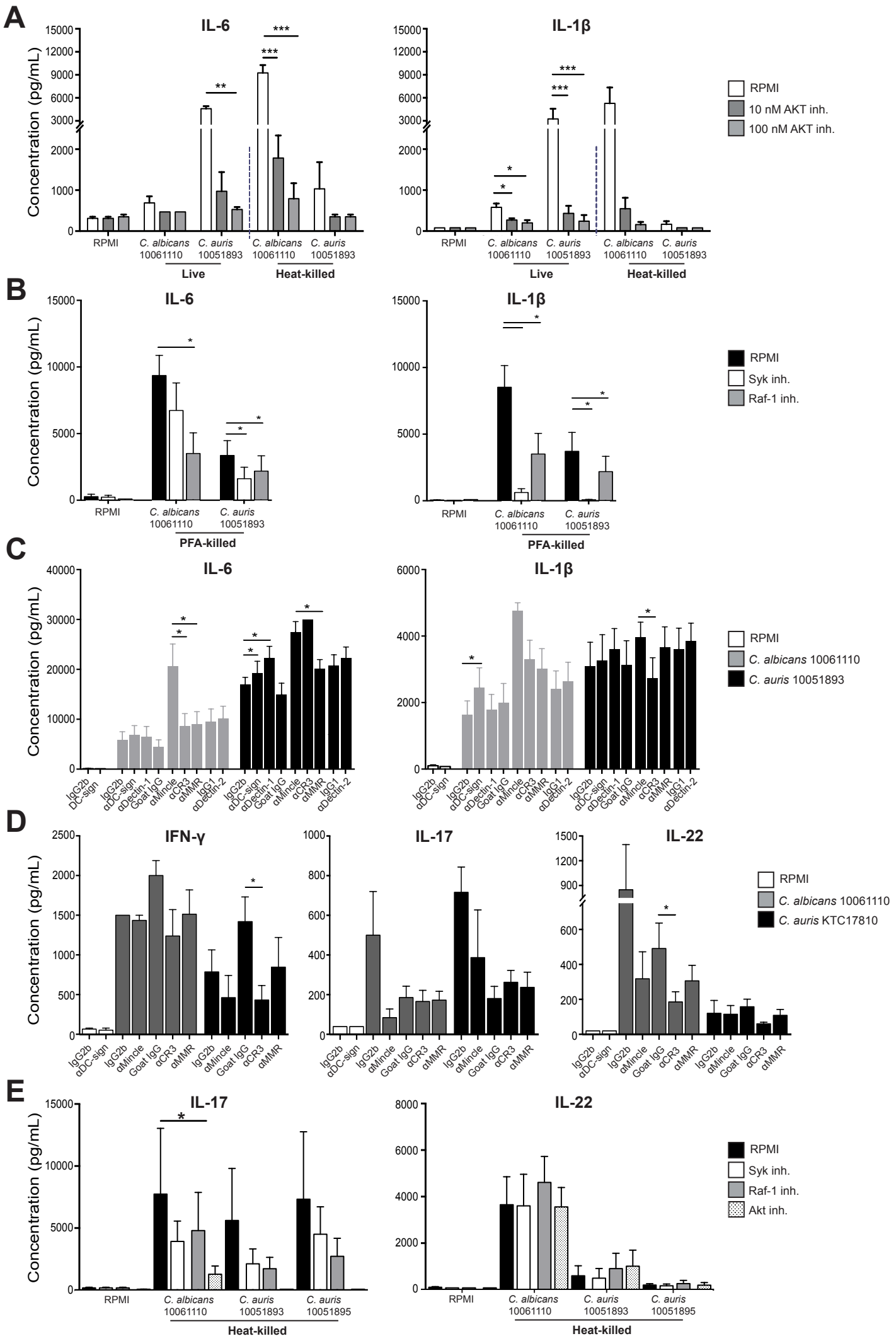
A
IL-6
IL-1β
Concentration (pg/mL)
RPMI
C. albicans 10061110
C. auris 10051893
Live
Heat-killed
RPMI
10 nM AKT inh.
100 nM AKT inh.
B
IL-6
IL-1β
PFA-killed
RPMI
Syk inh.
Raf-1 inh.
C
IL-6
IL-1β
IgG2b
DC-sign
αDC-sign
αDectin-1
Goat IgG
αMincle
αCR3
αMMR
IgG1
αDectin-2
RPMI
C. albicans 10061110
C. auris 10051893
D
IFN-γ
IL-17
IL-22
RPMI
C. albicans 10061110
C. auris KTC17810
E
IL-17
IL-22
C. auris 10051895
Akt inh.

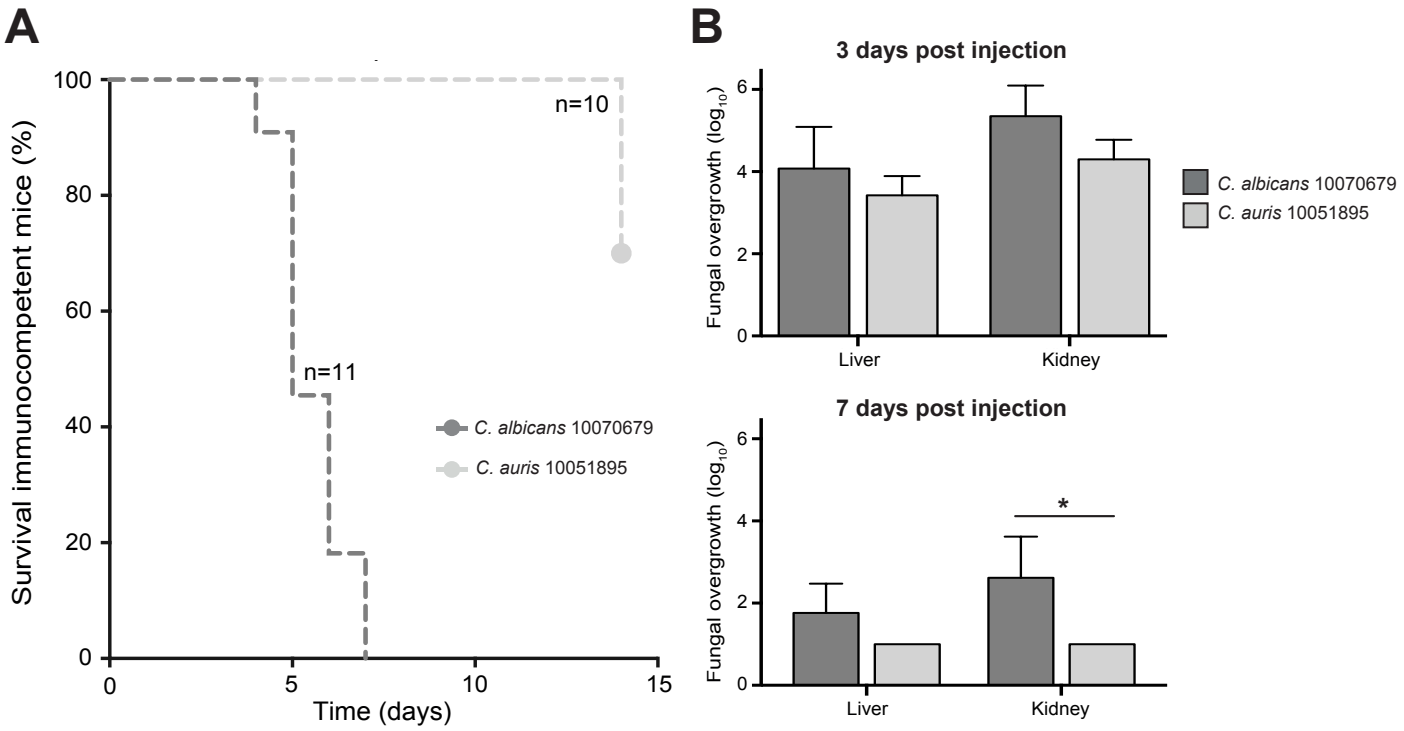
A
Survival immunocompetent mice (%)
100
80
60
40
20
0
0
5
10
15
Time (days)
n=10
n=11
C. albicans 10070679
C. auris 10051895
B
3 days post injection
Fungal overgrowth (log10)
6
4
2
0
Liver
Kidney
C. albicans 10070679
C. auris 10051895
7 days post injection
Fungal overgrowth (log10)
6
4
2
0
*
Liver
Kidney

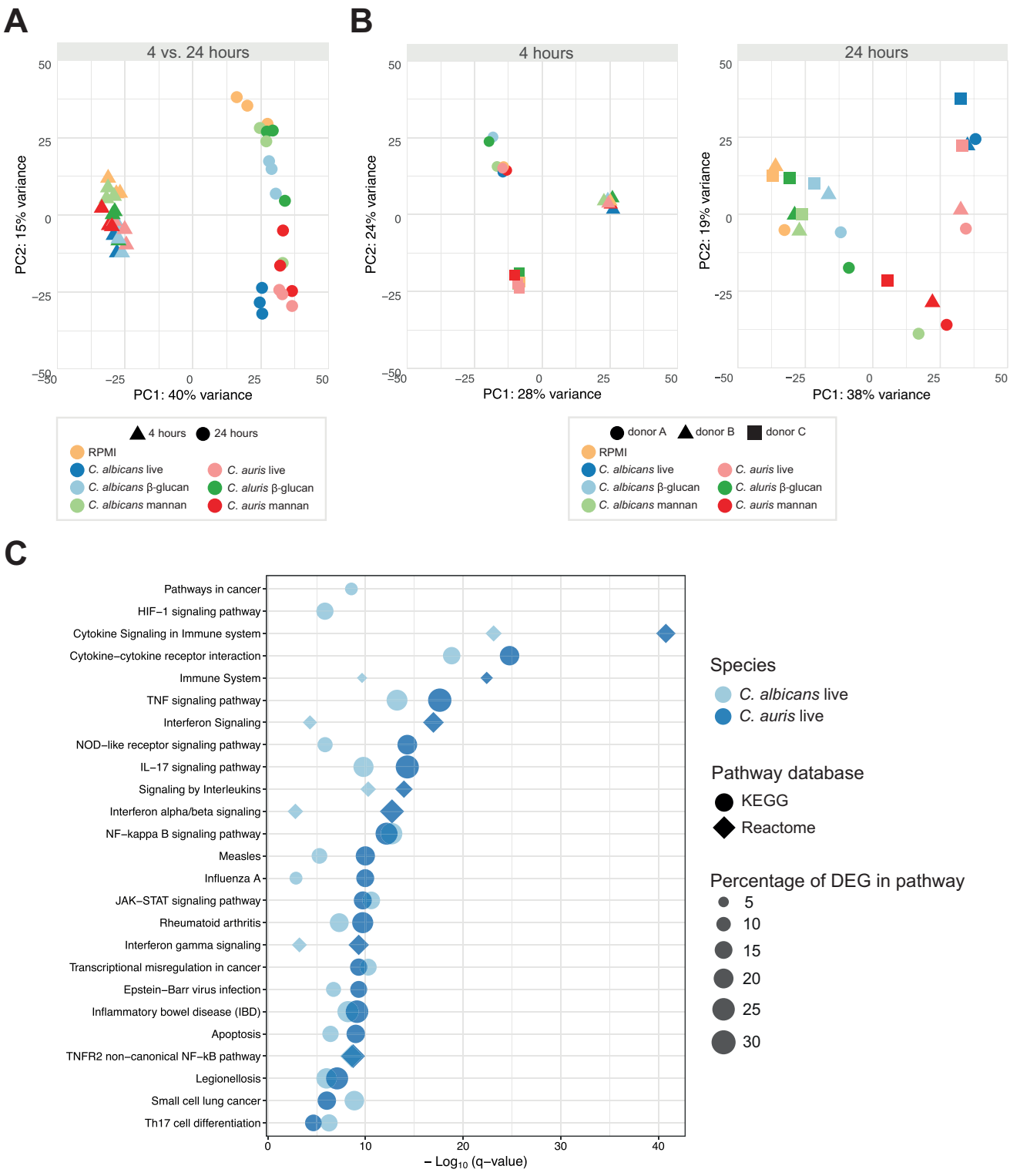

Figure S1 | Transcriptomic profiling PBMCs stimulated with live C. albicans or C. auris and respective cell wall components β-glucans and mannans for 4 and 24 hours. Related to Figure 1 and 3. (A) PCA of normalized data displaying the variance of conditions to each stimulus (color) and time-point (shape). (B) PCA displaying the variance at 4 (left panel) and 24-hours (right panel) for each stimulus (color) and donor (shape). (C) Pathway enrichment plot displaying the top 20 enriched pathways for both C. albicans live and C. auris live (color) at 24 hours. Enrichment determined using Consensus PathDB, including pathways as defined by KEGG and Reactome (shape), considering a q-value < 0.01 significant. Size of the geometric points indicates the amount of DEG in relation to the pathways' size.

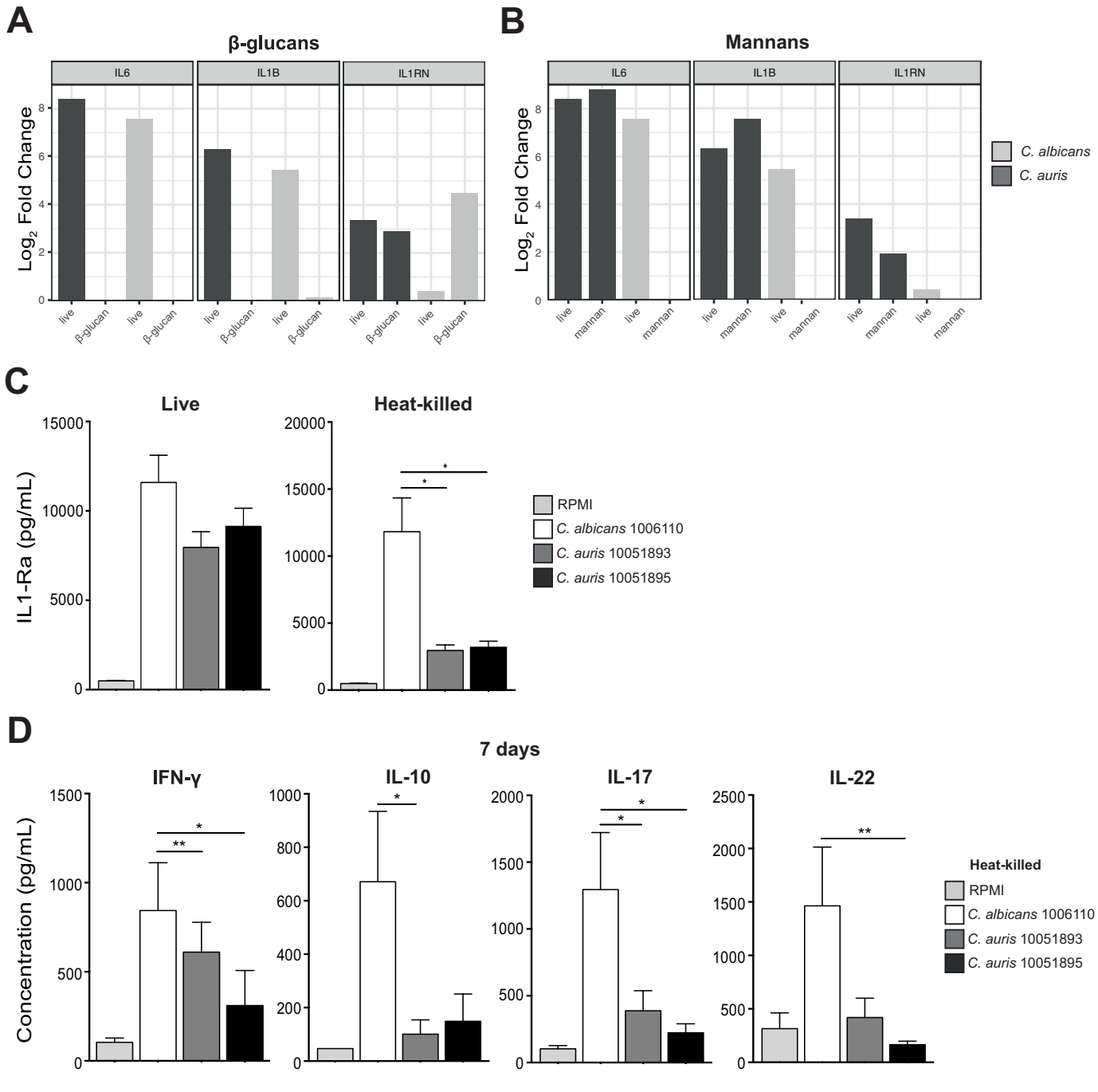

Figure S2 | Comparative innate host immune response between *C. albicans* and *C. auris*. Related to Figure 2 and 3. (A) Log_2Fold Change of *IL-6*, *IL-1β* and *IL-1RN* (encoding for IL-1Ra) gene expression in PBMCs stimulated for 24 hours with *C. albicans* and *C. auris*, and their respective purified β-glucans. (B) Log_2Fold Change of *IL-6*, *IL-1β* and *IL-1RN* (encoding for IL-1Ra) gene expression in PBMCs stimulated for 24 hours with *C. albicans* and *C. auris*, and their respective purified mannans. (C) PBMC production of cytokines IL-1Ra after stimulation without (RPMI; negative control) or with live or heat-killed *C. albicans* and *C. auris* for 24 hours. (D) PBMC production of cytokines IFN-γ, IL-10, IL-17 and IL-22 after stimulation without (RPMI; negative control) or with heat-killed *C. albicans* and *C. auris* for 7 days.

Graphs represent mean ± SEM, n = 6 – 12, pooled from two to four independent experiments. * $p < 0.05$, *** $p < 0.001$, Wilcoxon signed-rank test.

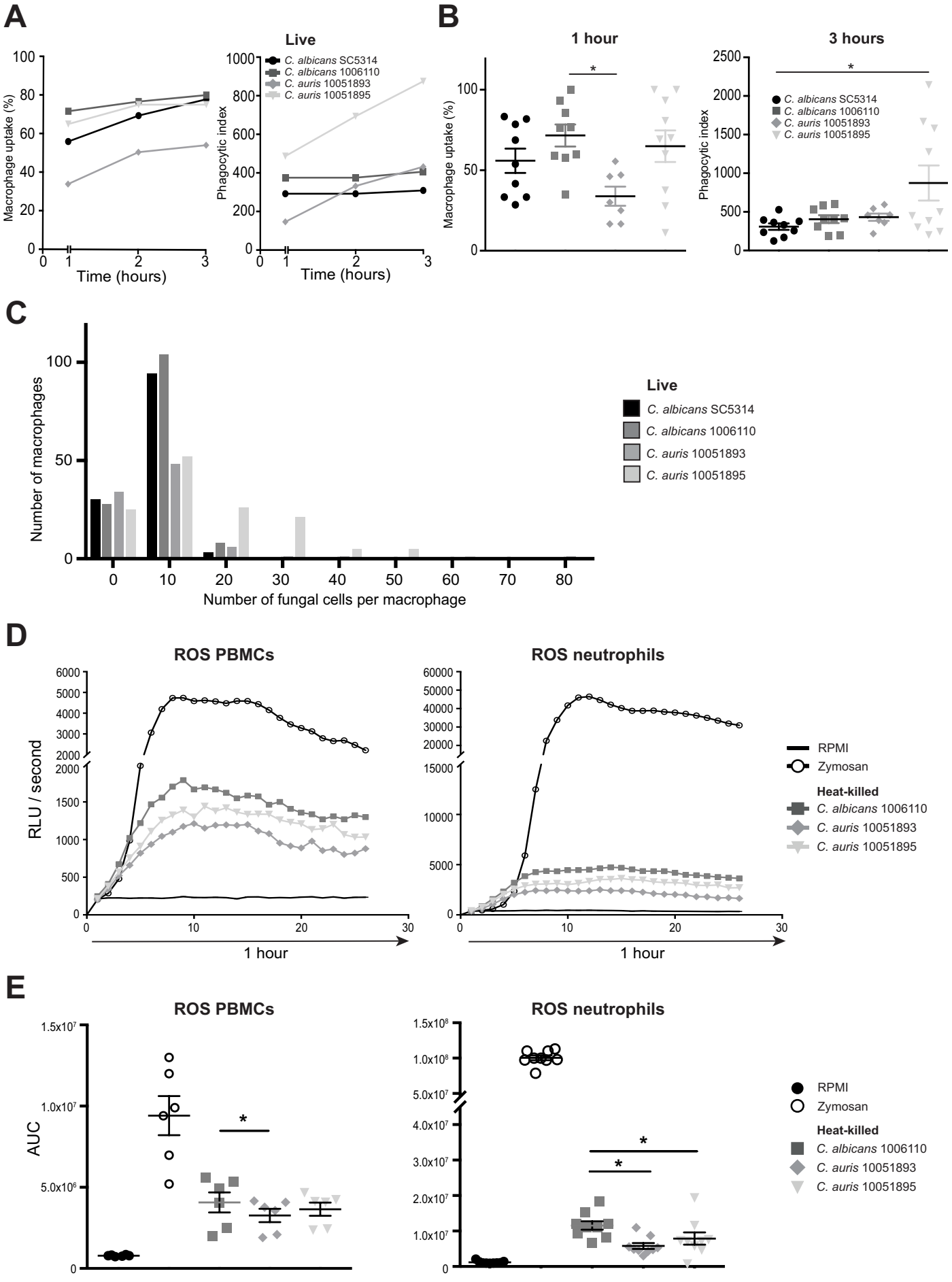

Figure S3 | Phagocytosis dynamics and ROS production of *C. auris* compared to *C. albicans*. Related to Figure 2. (A) The BMDM phagocytic capacity of live *C. albicans* or *C. auris* conidia strains in a 3-hour period. BMDM engulfment, depicted as the percentage of macrophages having phagocytosed at least one fungal cell (left). Phagocytic index, considered the number of fungal

cells engulfed per 100 macrophages (right). (B) The BMDM phagocytic capacity of live *C. albicans* or *C. auris* conidia strains. 1-hour BMDM engulfment, depicted as the percentage of macrophages having phagocytosed at least one fungal cell (left). 3-hour BMDM phagocytic index, considered the number of fungal cells engulfed per 100 macrophages (right). (C) Distribution of phagocytosed live cells per macrophage in a period of 3 hours. (D) 1-hour time-course of ROS production of PBMCs (left) and neutrophils (right) monitored directly after stimulation without (RPMI; negative control) or with Zymosan (positive control), or heat-killed *C. albicans* and *C. auris*, depicted as area of light units (RLU) per second. (E) Luminol oxidation as measure of ROS production of PBMCs (left) and neutrophils (right) monitored directly after stimulation without (RPMI; negative control) or with Zymosan (positive control), or heat-killed *C. albicans* and *C. auris*, depicted as area under the curve of relative of RLU / second.
Graphs represent mean ± SEM, n = 6 – 12, pooled from two to four independent experiments. * $p < 0.05$, *** $p < 0.001$, 1-way ANOVA (B), Wilcoxon signed-rank test (E).

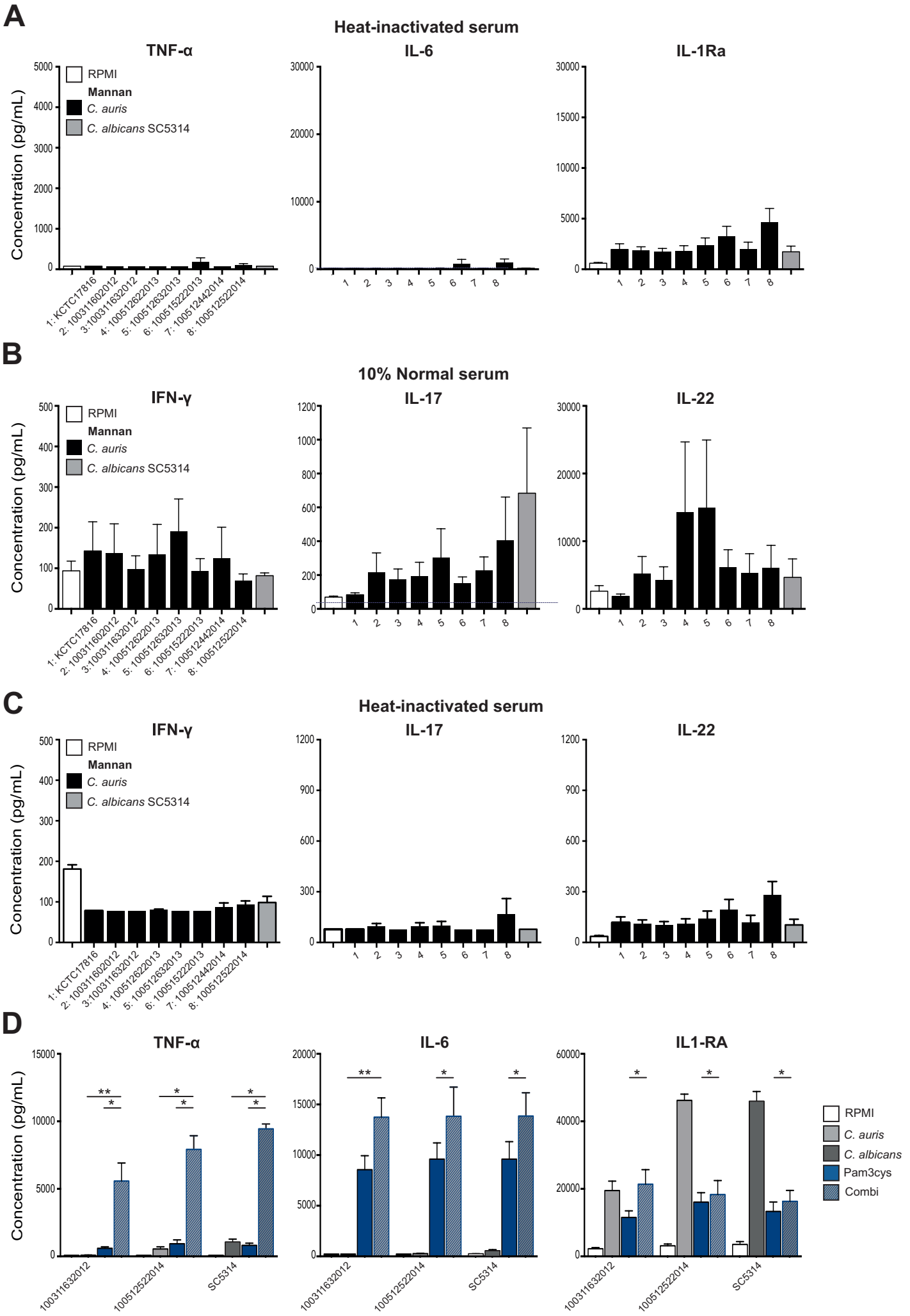
A
Heat-inactivated serum
TNF-α
IL-6
IL-1Ra
Concentration (pg/mL)
RPMI
Mannan
C. auris
C. albicans SC5314
1: KCTC17816
2: 100311602012
3:100311632012
4: 100512622013
5: 100512632013
6: 100515222013
7: 100512442014
8: 100512522014
B
10% Normal serum
IFN-γ
IL-17
IL-22
C
Heat-inactivated serum
IFN-γ
IL-17
IL-22
D
TNF-α
IL-6
IL1-RA
100311632012
100512522014
SC5314
RPMI
C. auris
C. albicans
Pam3cys
Combi

Figure S4 | Comparative innate host immune response between opsonized and non-opsonized *C. albicans* and *C. auris* and respective cell wall components. Related to Figure 4. (A) PBMC production of cytokines TNF-α, IL-6 and IL-1RA after 24-hour stimulation without (RPMI; negative control) or with purified mannans from □*albicans* and various C. auris strains in the presence of 10% heat-inactivated serum. Statistical testing was performed on cytokine levels for each *C. auris* strain in comparison to *C. albicans* SC5314. (B-C) PBMC production of cytokines IFN-γ, IL-17 and IL-22 after 7 days of stimulation without (RPMI; negative control) or with purified mannans from *C. albicans* and various *C. auris* strains in the presence of 10% normal serum (B) or 10% heat-inactivated serum (C). Statistical testing was performed on cytokine levels for each *C. auris* strain in comparison to *C. albicans* SC5314. (D) PBMC production of cytokines TNFα, IL-6 and IL-1Ra after 24-hour stimulation without (RPMI; negative control) or with Pam3cys and/or purified β-glucans from different *C. auris* and *C. albicans* strains in the presence of 10% human serum.
Graphs represent mean ± SEM, n = 6 – 12, pooled from two to four independent experiments. * $p < 0.05$, *** $p < 0.001$, Wilcoxon signed-rank test.

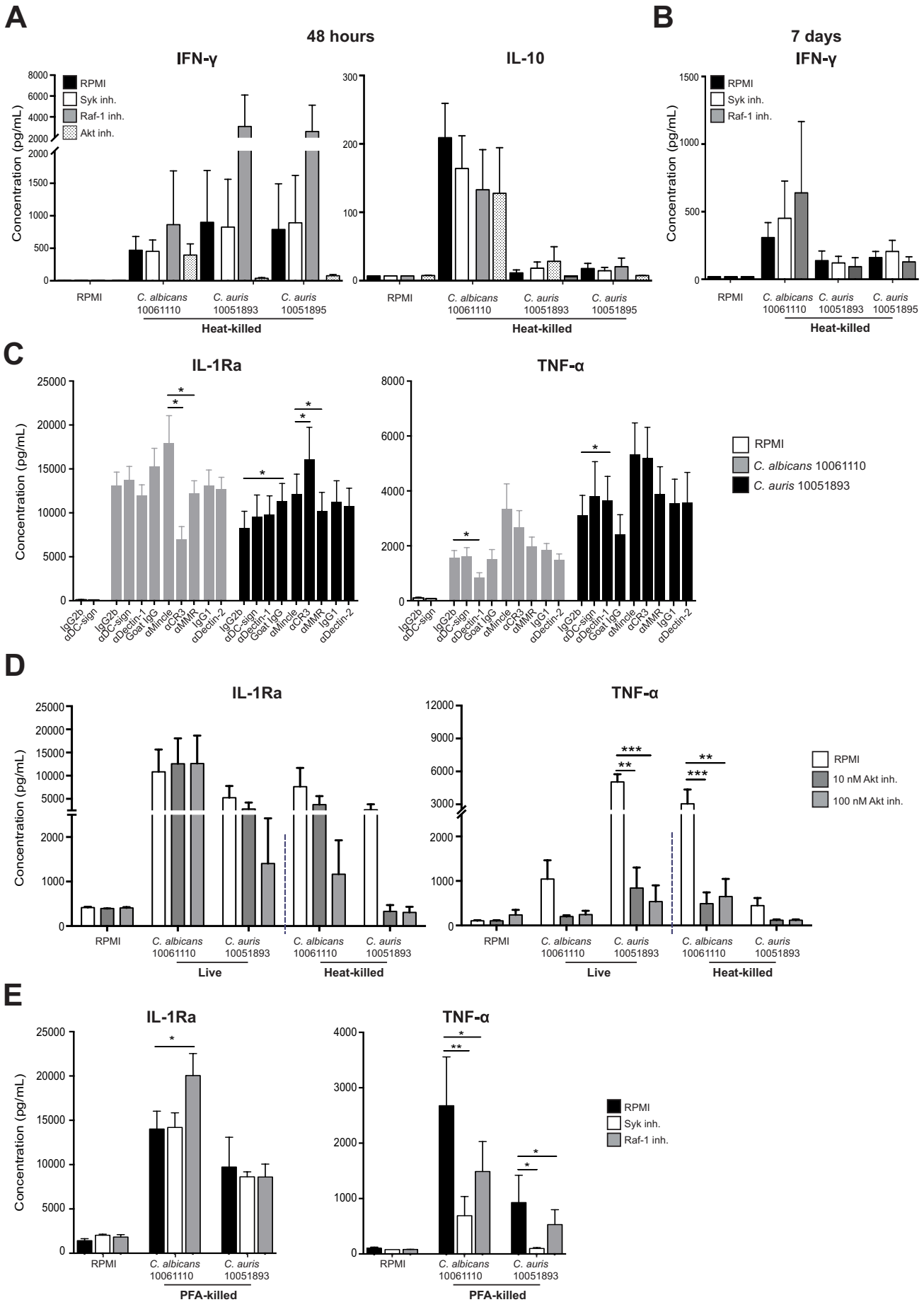

Figure S5 | The effect of blocking PRR and signaling pathways on the *C. albicans* and *C. auris* induced cytokine production. Related to Figure 5. (□PBMC production of cytokines IFN-γ and IL-10 after 48-hour stimulation without (RPMI; negative control) or with heat-killed □*albicans* and *C. auris*, subjected to RPMI or a 1-hour pre-incubation with Syk, Raf-1 or Akt inhibitors. (B) PBMC production of cytokines IFN-γ after 7 days of stimulation without (RPMI; negative control) or with heat-killed *C. albicans* and *C. auris*, subjected to RPMI or a 1-hour pre-incubation with Syk, Raf-1 or Akt inhibitors. (C) PBMC production of cytokines IL-1Ra and TNF-α

after 24-hour stimulation without (RPMI; negative control) or with live □*albicans* and *C. auris*, subjected to a 1-hour pre-incubation □IgG2b, Goat IgG and IgG1 control isotype antibodies, or DC-SIGN, Dectin-1, Mincle, MMR, CR3 and Dectin-2 blocking antibodies. Cytokine levels were compared between the neutralizing antibodies and the correspondent isotype controls. (D) PBMC production of cytokines IL-1Ra and TNF-α after 24-hour stimulation without (RPMI; negative control) or with live or heat-killed *C. albicans* and *C. auris*, subjected to RPMI or a 1-hour pre-incubation with the PI3K/Akt inhibitor wortmannin. (E) PBMC production of cytokines IL-1Ra and TNF-α after 24-hour stimulation without (RPMI; negative control) or with PFA-killed *C. albicans* and *C. auris*, subjected to RPMI or a 1-hour pre-incubation with the Syk inhibitor R406 or Raf-1 inhibitor GW5074.

Graphs represent mean ± SEM, n = 3 – 12, pooled from two to four independent experiments. * $p < 0.05$, *** $p < 0.001$, Wilcoxon signed-rank test.